NASA MEMO 4-20-59L

NASA

MEMORANDUM

TRANSONIC AERODYNAMIC CHARACTERISTICS OF A 45° SWEPT-WING—FUSELAGE MODEL WITH A FINNED AND UNFINNED BODY PYLON-MOUNTED BENEATH THE FUSELAGE OR WING, INCLUDING MEASUREMENTS OF BODY LOADS

By Dewey E. Wornom

Langley Research Center
Langley Field, Va.

Declassified May 29, 1961

NATIONAL AERONAUTICS AND SPACE ADMINISTRATION
WASHINGTON
May 1959

NATIONAL AERONAUTICS AND SPACE ADMINISTRATION

MEMORANDUM 4-20-59L

TRANSONIC AERODYNAMIC CHARACTERISTICS OF A 45° SWEPT-WING—FUSELAGE MODEL WITH A FINNED AND UNFINNED BODY PYLON-MOUNTED BENEATH THE FUSELAGE OR WING, INCLUDING MEASUREMENTS OF BODY LOADS

By Dewey E. Wornom

SUMMARY

An investigation of a model of a standard size body in combination with a representative 45° swept-wing—fuselage model has been conducted in the Langley 8-foot transonic pressure tunnel over a Mach number range from 0.80 to 1.43. The body, with a fineness ratio of 8.5, was tested with and without fins, and was pylon-mounted beneath the fuselage or wing. Force measurements were obtained on the wing-fuselage model with and without the body, for an angle-of-attack range from -2° to approximately 12° and an angle-of-sideslip range from -8° to 8°. In addition, body loads were measured over the same angle-of-attack and angle-of-sideslip range. The Reynolds number for the investigation, based on the wing mean aerodynamic chord, varied from 1.85×10^6 to 2.85×10^6.

The addition of the body beneath the fuselage or the wing increased the drag coefficient of the complete model over the Mach number range tested. On the basis of the drag increase per body, the under-fuselage position was the more favorable. Furthermore, the bodies tended to increase the lateral stability of the complete model.

The variation of body loads with angle of attack for the unfinned bodies was generally small and linear over the Mach number range tested with the addition of fins causing large increases in the rates of change of normal-force coefficient and nose-down pitching-moment coefficient. The variation of body side-force coefficient with sideslip for the unfinned body beneath the fuselage was at least twice as large as the variation of this load for the unfinned body beneath the wing. The addition of fins to the body beneath either the fuselage or the

wing approximately doubled the rate of change of body side-force coefficient with sideslip. Furthermore, the variation of body side-force coefficient with sideslip for the body beneath the wing was at least twice as large as the variation of this load with angle of attack.

INTRODUCTION

A finned body of standard size, shape, and lug position as determined by the Wright Aeronautical Development Command has been considered for external installation on current and future fighter-bomber type airplanes. In order to investigate the body forces and moments within the operating speed range of these airplanes, tests of the body attached to a representative wing-fuselage combination were performed in the Langley 8-foot transonic pressure tunnel. The body was of 0.07-scale with a maximum diameter of 1.40 inches and a fineness ratio of 8.5. The wing chosen for the investigation was swept back 45° at the quarter-chord line, with an aspect ratio of 4.0 and a taper ratio of 0.15. The ratio of wing area to body frontal area is 131.5.

Tests were made of three different configurations: the wing-fuselage combination alone, the wing-fuselage combination with one body pylon-mounted beneath the fuselage center line, and the wing-fuselage combination with a body pylon-mounted under each wing panel. Forces and moments were measured simultaneously and separately on the bodies and the wing-fuselage combination with and without bodies at Mach numbers from 0.80 to 1.43 over an angle-of-attack and angle-of-sideslip range.

Reynolds number for the investigation, based on the wing mean aerodynamic chord, varied from approximately 1.85×10^6 to 2.85×10^6.

Additional data involving body loads for a body mounted beneath a swept wing can be found in references 1 to 6.

SYMBOLS

The systems of axes used for data presentation, stability axes for the wing-fuselage combination (with or without bodies), and body axes for the bodies proper are shown in figure 1.

A	maximum frontal area of body, 0.01069 sq ft
b	wing span, in.
C_D	wing-fuselage drag coefficient, $\frac{Drag}{qS}$

$C_{D'}$ wing-fuselage longitudinal-force coefficient, $\frac{\text{Longitudinal force}}{qS}$, ($C_{D'} = C_D$ when $\beta = 0^\circ$)

C_L wing-fuselage lift coefficient, $\frac{\text{Lift}}{qS}$

C_l wing-fuselage rolling-moment coefficient, $\frac{\text{Rolling moment}}{qSb}$

C_m wing-fuselage pitching-moment coefficient, $\frac{\text{Pitching moment about } 0.25\bar{c}}{qS\bar{c}}$

C_n wing-fuselage yawing-moment coefficient, $\frac{\text{Yawing moment about } 0.25\bar{c}}{qSb}$

C_Y wing-fuselage lateral-force coefficient, $\frac{\text{Lateral force}}{qS}$

$C_{c,b}$ body axial-force coefficient, $\frac{\text{Body axial force}}{qA}$

$C_{m,b}$ body pitching-moment coefficient, $\frac{\text{Body pitching moment about } 0.435l}{qAl}$

$C_{N,b}$ body normal-force coefficient, $\frac{\text{Body normal force}}{qA}$

$C_{n,b}$ body yawing-moment coefficient, $\frac{\text{Body yawing moment about } 0.435l}{qAl}$

$C_{Y,b}$ body lateral-force coefficient, $\frac{\text{Body lateral force}}{qA}$

$C_{m_{C_L}}$ static longitudinal-stability parameter, averaged from $C_L = 0$ over linear portion of curve

C_{l_β} effective-dihedral derivative, $\partial C_l / \partial \beta$

C_{n_β} directional-stability derivative, $\partial C_n / \partial \beta$

C_{Y_β}	lateral-force derivative, $\partial C_Y / \partial \beta$
C_{L_α}	lift-curve slope per degree, averaged from $C_L = 0$ over linear portion of curve
c	local wing chord, in.
$\bar{c}$	wing mean aerodynamic chord, in.
l	length of body, in.
M	free-stream Mach number
q	free-stream dynamic pressure, lb/sq ft
R	Reynolds number based on $\bar{c}$
S	wing area, sq ft
y	spanwise distance from plane of symmetry of wing-fuselage model, in.
α	angle of attack, deg
β	angle of sideslip, deg

APPARATUS AND TESTS

Tunnel

The investigation was conducted in the Langley 8-foot transonic pressure tunnel, which is a single return system with a rectangular test section permitting continuous operation throughout the transonic speed range. For the supersonic Mach number of 1.43, filler blocks were installed in the slotted test section as described in reference 7. Automatic stagnation-temperature controls maintain a constant and uniform temperature of 120° F during the test. In order to prevent condensation, the dewpoint was maintained at 0° F or lower.

Through design of the sting-support system, the model is essentially located at the center line of the test section throughout the ranges of angle-of-attack and angle-of-sideslip tested.

Model

Dimensions of the wing-fuselage combination are presented in figures 2(a) and 2(b). The steel wing was cambered for a design lift coefficient of 0.2. It had 45° of sweepback at the quarter-chord line, an aspect ratio of 4.0, and a taper ratio of 0.15. The wing airfoil section varied from NACA 64A206 at the root to NACA 64A203, a = 0.8 (modified), at 0.50b/2 and remained the same out to the tip. The fuselage, constructed of steel with a plastic exterior, was cambered and indented for a design Mach number of 1.43 in order to reduce drag due to lift and wave drag. (See ref. 8.) Fuselage coordinates are given in table I.

Body dimensions are shown in figure 2(c). The body was a 0.07-scale model made of aluminum with a length of 11.90 inches, a maximum diameter of 1.40 inches, and a fineness ratio of 8.5. Coordinates of the body are given in table II. The pylon, which was used in all body positions, was unswept, had a 65A005 airfoil section, and was positioned with respect to the body as shown in figure 2(c). The lower end of the pylon was attached to the bottom of the body by means of an internal balance. A slot in the top of the body provided clearance between the body and the pylon of approximately 1/32 of an inch.

For all positions, the longitudinal location of the body center of gravity (0.435l) was 0.12$\bar{c}$ rearward of the quarter-chord point of the wing mean aerodynamic chord. The vertical distance between the body center line and adjacent wing or fuselage surface was 1.10 inches (0.786 of the maximum body diameter) as shown in figures 2(a) and 2(b).

Photographs of the model installed in the test section of the 8-foot transonic pressure tunnel are shown in figure 3.

Measurements and Accuracies

Forces and moments were measured on the wing-fuselage combination, with or without bodies, by a six-component electrical strain-gage balance mounted within the fuselage. Simultaneously, but independently, the forces and moments on the bodies proper were measured by a five-component electrical strain-gage balance mounted within the bodies. In the case of the bodies under the wing, the balance was located within the body under the left wing. Wing-fuselage-combination force and moment coefficients were based on the wing area of 1.408 square feet, mean aerodynamic chord of 8.421 inches, and were adjusted for base drag. Body force and moment coefficients were based on the body maximum cross-sectional area of 0.01069 square foot and length of 11.9 inches.

Through consideration of the static calibrations of the electrical strain-gage balances and repeatability of data, the estimated accuracy of the coefficients for a Mach number of 0.80 and a tunnel stagnation pressure of 0.75 atmosphere is as follows:

C_L	±0.01	$C_{N,b}$	±0.04
C_D	±0.001	$C_{c,b}$	±0.014
C_m	±0.002	$C_{m,b}$	±0.014
C_l	±0.0003	$C_{n,b}$	±0.01
C_n	±0.0005	$C_{Y,b}$	±0.04
C_Y	±0.004		

Since the accuracy is inversely proportional to dynamic pressure, these values decrease with Mach number and tunnel stagnation pressure.

Angles of attack and sideslip were determined with a pendulum-type strain-gage unit, which was located within the nose of the fuselage and considered to be accurate to ±0.1 degree. Deflections due to loads on the bodies were not accounted for, but static-load-calibration data showed that body deflections due to maximum loads experienced during tests would be less than 0.5 degree. A dummy balance in the body beneath the right wing insured that deflections due to loads were identical to those of the body beneath the left wing with the internal balance.

Tests

Tests were made at Mach numbers from 0.80 to 1.43 over an angle-of-attack range from -2° to approximately 12° and an angle-of-sideslip range from -8° to 8°. In some cases, load limits of the internal strain-gage balance reduced the maximum angles. The lateral tests, with angle of sideslip varying, were made at angles of attack of approximately 0° and 5°. In order to obtain desired angle range without exceeding balance limits, the tunnel stagnation pressure was reduced on certain tests. For the longitudinal tests at Mach numbers from 0.80 to 1.20, the tunnel pressure was reduced to 0.9 atmosphere, and for the lateral tests over the same Mach number range, the tunnel pressure was reduced to 0.75 atmosphere. (See fig. 4.) Data for the Mach number of 1.43 were taken at a tunnel pressure of 0.65 atmosphere with the exception of the data obtained with the finned body beneath the fuselage. For this configuration, data were taken at 1.0 atmosphere. Comparison of low angle data at 1.0 and 0.65 tunnel atmosphere for other configurations of this investigation (not presented herein) shows no appreciable Reynolds number effect on the forces and moments.

For transition, 1/8-inch-wide strips of No. 120 carborundum grit (maximum diameter of 0.0049 in.), sparsely applied, were used on the upper and lower wing surfaces and on the fuselage nose and body nose at 10 percent of their respective lengths.

RESULTS

The data from this investigation are presented in the following figures:

	Figure
Complete model -	
Effects of transition on the longitudinal characteristics with finned body pylon-mounted beneath the fuselage	5
Longitudinal characteristics of model without bodies	6
Longitudinal characteristics with finned and unfinned body pylon-mounted beneath the fuselage	7
Longitudinal characteristics with finned and unfinned bodies pylon-mounted beneath the wing	8
Lateral characteristics of model without bodies	9
Lateral characteristics with finned and unfinned body pylon-mounted beneath the fuselage	10
Lateral characteristics with finned and unfinned bodies pylon-mounted beneath the wing	11
Body loads -	
Variation with angle of attack for the finned and unfinned body pylon-mounted beneath the fuselage	12
Variation with angle of attack for the finned and unfinned bodies pylon-mounted beneath the left wing	13
Variation with angle of sideslip for the finned and unfinned body pylon-mounted beneath the fuselage	14
Variation with angle of sideslip for the finned and unfinned body pylon-mounted beneath the left wing	15
Analysis -	
Variation with Mach number of the longitudinal characteristics of the swept wing-fuselage configuration with and without bodies	16
Variation with Mach number of the lateral characteristics of the swept wing-fuselage configuration with and without bodies	17
Variation with Mach number of body loads for the bodies pylon-mounted beneath the fuselage or wing with or without fins	18 to 21

In order to assist the reader in the use of the figures, a small front view of the particular configuration has been placed at the top of each figure. A completely darkened view, such as the one shown on figure 7, indicates that the data were obtained by means of the balance within the fuselage which measured the forces and moments on the complete configuration. A view, such as the one shown on figure 13 in which just the body is darkened, indicates that the data were obtained by means of the balance within that body which measured the forces and moments on the body proper in the presence of the wing-fuselage combination and pylon.

The use of staggered scales has been employed extensively in the presentation of the data, and care should be exercised in the selection of the zero axis for each curve.

DISCUSSION

Complete Model Characteristics

Effect of model transition.- Addition of transition strips had no appreciable effect on the lift or pitching-moment characteristics. (See fig. 5.) An increase of approximately 0.0025 in drag coefficient at zero and low lifts is noted over the Mach number range tested but slowly vanished with an increase in lift coefficient to the maximum test lift coefficient of approximately 0.6.

Effect of bodies on longitudinal characteristics.- The most significant effect of either the body beneath the fuselage or two bodies beneath the wing was on the drag characteristics as shown in figure 16. At transonic speeds, the increase in wave drag due to the bodies beneath the wing was approximately three times greater than that for the body beneath the fuselage. For $C_L = 0.3$ and above subsonic speeds, the total drag increase due to the bodies beneath the wing is more than double that due to the body beneath the fuselage. Based on the drag increment per body, the fuselage position appears to be more favorable than the wing position. It should be noted, however, that a more forward chordwise position of the bodies beneath the wing might result in less total drag as indicated in reference 9. Addition of fins to the bodies had no further effect on the drag characteristics of the complete model.

The addition of the bodies resulted in a slight reduction in lift coefficient with an appreciable attendant effect on the pitching-moment coefficient. (See figs. 6, 7, and 8.) The pitching-moment coefficient was increased by approximately 0.01 to 0.03 over the test Mach number range and lift-coefficient range, with the bodies beneath the wing

having the greatest effect. The only appreciable effect of the addition of fins is noted for the bodies beneath the wing whereby the pitching-moment coefficient was increased negatively by approximately 0.006 at subsonic speeds.

Effect of bodies on the lateral characteristics.- In general, the addition of the bodies tended to increase the lateral stability of the complete model at $\alpha \approx -0.2^\circ$ and 5.7°, with the most pronounced effect being upon the effective dihedral Cl_β above a Mach number of 0.95 at $\alpha \approx -0.2^\circ$ (fig. 17). Addition of the fins to the bodies had no further effect on the lateral characteristics.

Body Loads

Effect of angle of attack.- For the unfinned body mounted beneath either the fuselage or the wing, the variation of body loads with α was generally small and linear over the Mach number range tested (figs. 12, 13, 18, and 19). An exception is shown, however, by the variations with α of $C_{Y,b}$ and $C_{n,b}$ for the body beneath the left wing. Because the body side loads act in the direction of the least structural strength of the supporting pylon, they are of considerable importance. However, the well inboard position of the body beneath the wing is more favorable than a more outboard position since reference 2 indicates that a more outboard position would have considerably greater rates of change in $C_{Y,b}$ with α and greater side loads at larger angles of attack.

The addition of fins to the bodies caused large increases in $C_{N,b}$ and nose-down $C_{m,b}$ with increases in α (figs. 12, 13, 18, and 19). It should be noted that similar changes would be expected from adding fins to the body alone in a uniform flow field. The fins also had an appreciable effect on $C_{Y,b}$ and $C_{n,b}$ for the body beneath the left wing (fig. 13). In this case, the addition of fins displaced the curves of $C_{Y,b}$ plotted against α by approximately 0.15 (inboard) over the Mach number range with little effect on their slopes. This displacement, accompanied by an increase in negative yawing moment (nose outboard), is probably due to the inward flow of the wing wake acting on the fins.

It is of interest to note that because of their structural importance the side loads on the body beneath the fuselage (with or without fins) were essentially zero over the test Mach number and angle-of-attack range (fig. 12).

Effects of sideslip.- The effects of sideslip on the body loads for $\alpha \approx -0.2^\circ$ and 5.7° are shown in figures 14, 15, 20, and 21. Variation of $C_{Y,b}$ and $C_{n,b}$ with β was essentially linear for the body (with or without fins) beneath the fuselage or wing over the test Mach number range. The rate of change of $C_{Y,b}$ and $C_{n,b}$ with β for the unfinned body beneath the fuselage was approximately twice as large as those for the body beneath the wing (at $\alpha \approx 5.7^\circ$). Although the data are insufficient to support definite conclusions, it appears that the higher rate of change of side load with β for the body beneath the fuselage is the result of influence of the fuselage in accelerating the cross-flow component due to sideslip. Furthermore, the variation of $C_{Y,b}$ and $C_{n,b}$ with β for the unfinned body beneath the wing was at least twice as large as the variation of these loads with α over the complete test Mach number range. The addition of fins to the body beneath the fuselage or wing approximately doubled the rate of change of $C_{Y,b}$ with β and was partly because of the added side area of the fins. A reversal of slope of the variation of $C_{n,b}$ with β (indicating a center-of-pressure shift from ahead to well behind the body assumed center of gravity) is also noted because of addition of the fins to either the body beneath the fuselage or wing.

L
2
0
6

Both positive and negative increases in β caused large changes in $C_{N,b}$ in the direction of the weight of the body and nose-up changes in $C_{m,b}$. The magnitude of the changes was greater for the body under the fuselage than for the body under the wing. It is not unreasonable to suppose that the supporting pylon exerts considerable effect on these loads by blocking the cross-flow component due to β between the body and fuselage or wing. Although the data are incomplete for the body beneath the fuselage, the rate of change of $C_{N,b}$ with β appears relatively insensitive to the addition of fins or increases in α.

CONCLUSIONS

An investigation of a model of a standard size body in combination with a representative 45° swept-wing—fuselage model has been conducted in the Langley 8-foot transonic pressure tunnel. Force measurements obtained on the wing-fuselage model with and without the body and on the body proper in the presence of the wing-fuselage model indicate the following conclusions:

1. The addition of the body beneath the fuselage or wing increased the drag coefficient of the complete model over the Mach number range tested. On the basis of the drag increase per body, the under-fuselage position was more favorable.

2. Addition of the body beneath the fuselage or the wing tended to increase the lateral stability of the complete model.

3. The variation of body loads with angle of attack α for the unfinned bodies beneath the fuselage or wing was generally small and linear over the Mach number range tested. The addition of fins, however, caused large increases in the magnitude of the rates of change of body normal-force coefficient $C_{N,b}$ and body pitching-moment coefficient $C_{m,b}$ with α.

4. The variations of body side-force coefficient $C_{Y,b}$ and body yawing-moment coefficient $C_{n,b}$ with angle of sideslip β for the unfinned body beneath the fuselage were at least twice as large as the variations of these loads for the unfinned body beneath the wing. The addition of fins to the body beneath either the fuselage or the wing approximately doubled the rate of $C_{Y,b}$ with β.

5. The variations of $C_{Y,b}$ and $C_{n,b}$ with β for the unfinned body beneath the wing were at least twice as large as the variations of these loads with α.

Langley Research Center,
National Aeronautics and Space Administration,
Langley Field, Va., January 23, 1959.

REFERENCES

1. Alford, William J., Jr., and Silvers, H. Norman.: Investigation at High Subsonic Speeds of Finned and Unfinned Bodies Mounted at Various Locations From the Wings of Unswept- and Swept-Wing—Fuselage Models, Including Measurements of Body Loads. NACA RM L54B18, 1954.

2. Guy, Lawrence D.: Loads on External Stores at Transonic and Supersonic Speeds. NACA RM L55E13b, 1955.

3. Guy, Lawrence D., and Hadaway, William M.: Aerodynamic Loads on an External Store Adjacent to a 45° Sweptback Wing at Mach Numbers From 0.70 to 1.96, Including an Evaluation of Techniques Used. NACA RM L55H12, 1955.

4. Morris, Odell A.: Aerodynamic Forces and Moments on a Large Ogive-Cylinder Store at Various Locations Below the Fuselage Center Line of a Swept-Wing Bomber Configuration at a Mach Number of 1.61. NACA RM L56I25, 1957.

5. Geier, Douglas J., and Carlson, Harry W.: Measurement of Static Forces on Externally Carried Bombs of Fineness Ratio 7.1 and 10.5 in the Flow Field of a Swept-Wing Fighter-Bomber Configuration at a Mach Number of 1.6. NACA RM L56K30, 1957.

6. Bobbitt, Percy J., Carlson, Harry W., and Pearson, Albin O.: Calculation of External-Store Loads and Correlation With Experiment. NACA RM L57D30a, 1957.

7. Matthews, Clarence W.: An Investigation of the Adaptation of a Transonic Slotted Tunnel to Supersonic Operation by Enclosing the Slots With Fairings. NACA RM L55H15, 1955.

8. Whitcomb, Richard T.: Some Considerations Regarding the Application of the Supersonic Area Rule to the Design of Airplane Fuselages. NACA RM L56E23a, 1956.

9. Pearson, Albin O.: Transonic Investigation of Effects of Spanwise and Chordwise External Store Location and Body Contouring on Aerodynamic Characteristics of 45° Sweptback Wing-Body Configurations. NACA RM L57G17, 1957.

TABLE I.- FUSELAGE COORDINATES

Fuselage station, in.	Fuselage radius (upper half), in.	Fuselage radius (lower half), in.	Fuselage station, in.	Fuselage radius (upper half), in.	Fuselage radius (lower half), in.
0	0	0	18.0	1.140	1.726
.5	.178	.178	18.5	1.126	1.752
1.0	.288	.288	19.0	1.120	1.773
1.5	.375	.375	19.5	1.122	1.790
2.0	.460	.460	20.0	1.132	1.804
2.5	.537	.537	20.5	1.150	1.813
3.0	.610	.610	21.0	1.174	1.819
3.5	.680	.680	21.5	1.202	1.819
4.0	.743	.743	22.0	1.220	1.812
4.5	.803	.803	22.5	1.229	1.805
5.0	.860	.860	23.0	1.231	1.795
5.5	.913	.913	23.5	1.233	1.783
6.0	.965	.965	24.0	1.235	1.770
6.5	1.015	1.015	24.5	1.236	1.754
7.0	1.061	1.061	25.0	1.237	1.735
7.5	1.108	1.108	25.5	1.238	1.712
8.0	1.155	1.155	26.0	1.240	1.686
8.5	1.200	1.200	26.5	1.242	1.655
9.0	1.242	1.242	27.0	1.243	1.619
9.5	1.284	1.284	27.5	1.245	1.578
10.0	1.325	1.325	28.0	1.245	1.530
10.5	1.365	1.365	28.5	1.246	1.480
11.0	1.404	1.404	29.0	1.245	1.433
11.5	1.445	1.445	29.5	1.243	1.385
12.0	1.479	1.479	30.0	1.236	1.339
12.5	1.495	1.505	30.5	1.224	1.292
13.0	1.491	1.530	31.0	1.207	1.248
13.5	1.475	1.550	31.5	1.187	1.204
14.0	1.435	1.568	32.0	1.158	1.158
14.5	1.393	1.585	32.5	1.118	1.118
15.0	1.351	1.601	33.0	1.076	1.076
15.5	1.310	1.619	33.5	1.031	1.031
16.0	1.266	1.636	34.0	.984	.984
16.5	1.226	1.654	34.5	.932	.932
17.0	1.192	1.675	35.0	.878	.878
17.5	1.162	1.700	35.3	.844	.844

TABLE II.- BODY COORDINATES

Body station, in.	Body radius, in.
0	0
.006	.029
.025	.053
.035	.060
.052	.069
.070	.077
.170	.123
.295	.174
.420	.218
.770	.326
1.120	.411
1.470	.473
1.820	.524
2.170	.565
2.520	.600
2.870	.630
3.220	.657
3.570	.681
3.920	.694
4.27 to 5.95	.700
6.300	.697
6.650	.689
7.000	.675
7.350	.656
7.700	.632
8.050	.604
8.400	.573
8.750	.557
9.100	.499
9.450	.457
9.800	.414
10.150	.368
10.500	.322
10.850	.276
11.200	.230
11.550	.187
11.900	.137

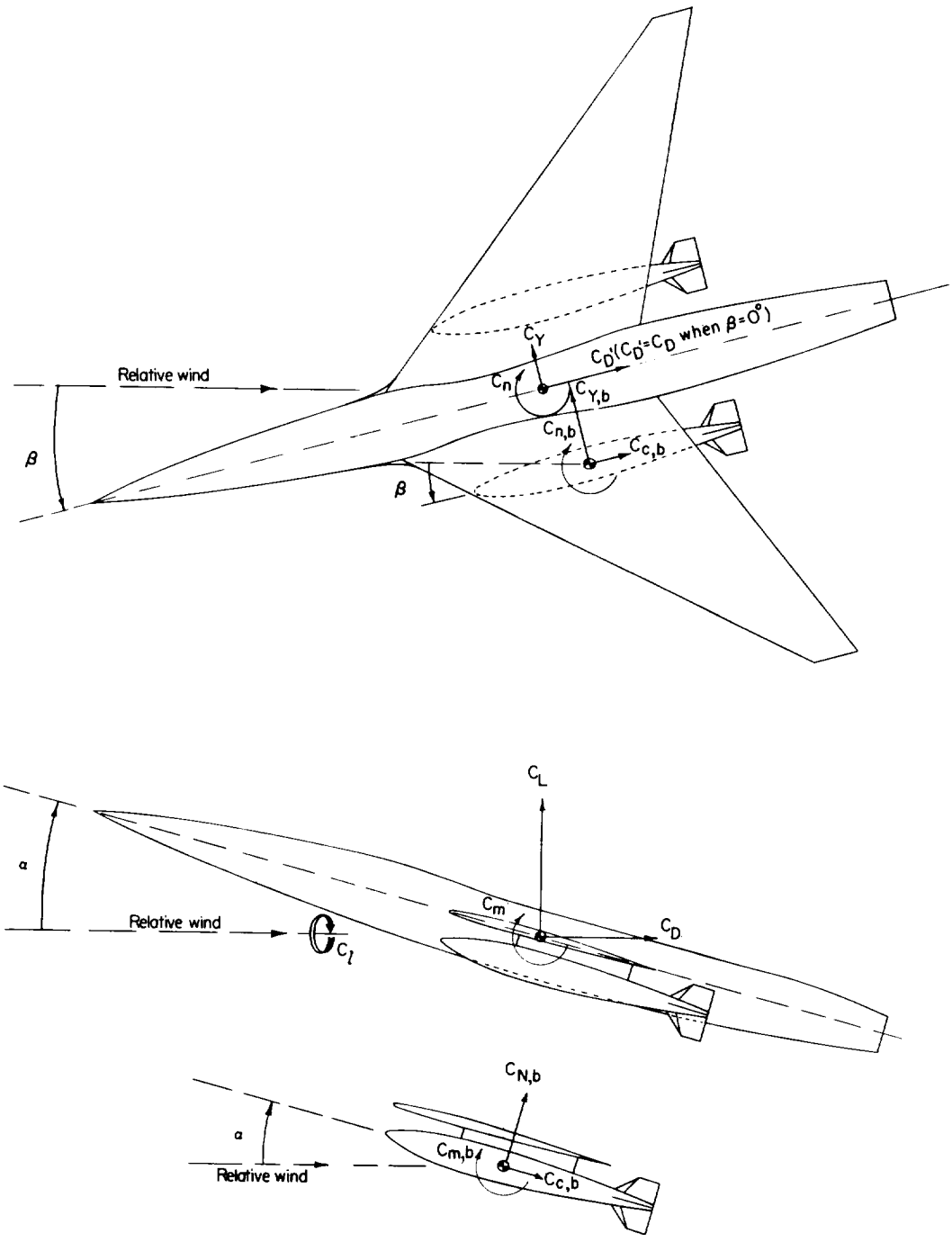

Figure 1.- Systems of axes for the wing-fuselage configuration and bodies. Arrows denote positive direction of force, moment, and angular measurements.

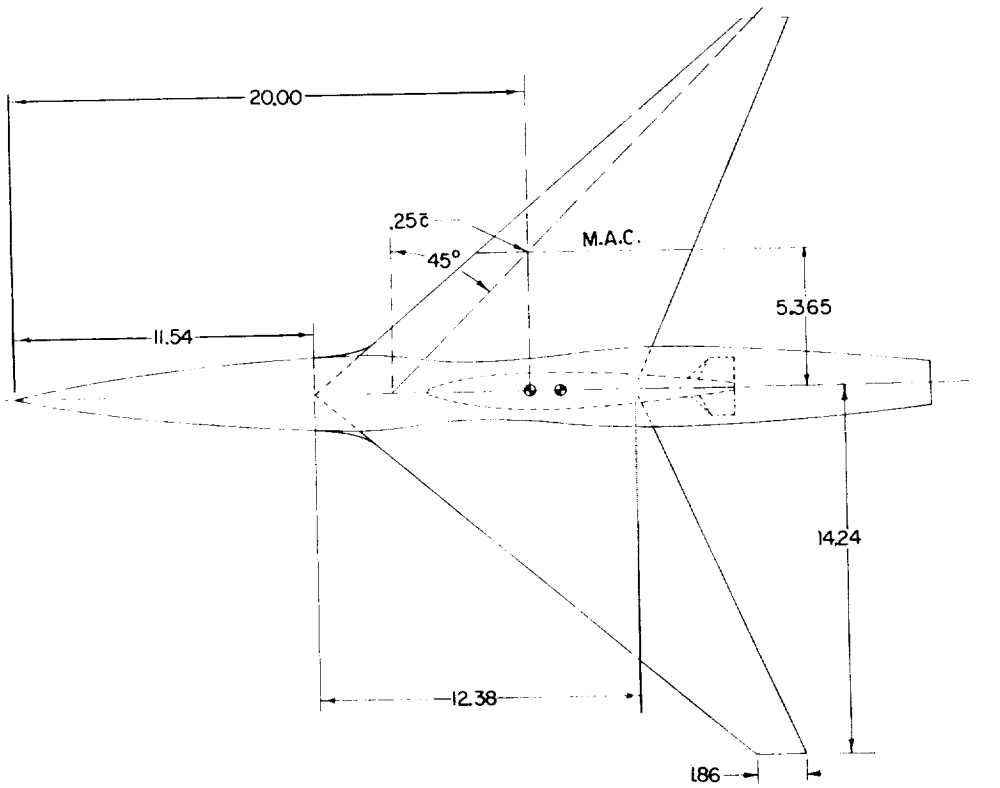

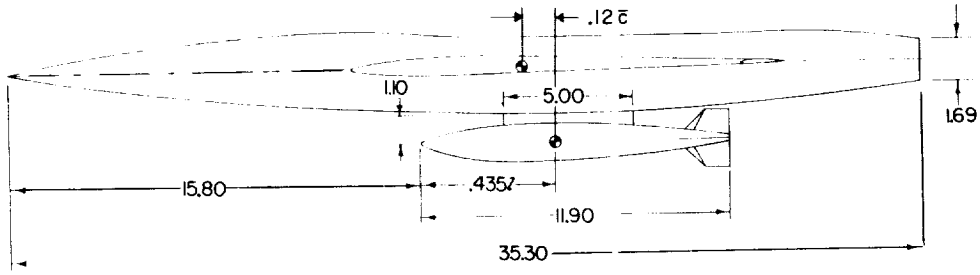

Wing details

Area, sq ft	1.408	2y/b = 0; NACA 64A206; a = 0
M.A.C., in.	8.421	2y/b = 0.50; NACA 64A203; a = 0.8 (modified)
Aspect ratio	4.0	2y/b = 1.0; NACA 64A203; a = 0.8 (modified)
Taper ratio	.15	
Dihedral, deg	0	

(a) Swept-wing—fuselage configuration with body pylon-mounted beneath the fuselage.

Figure 2.- Detail drawings of model investigated. All dimensions in inches unless otherwise noted.

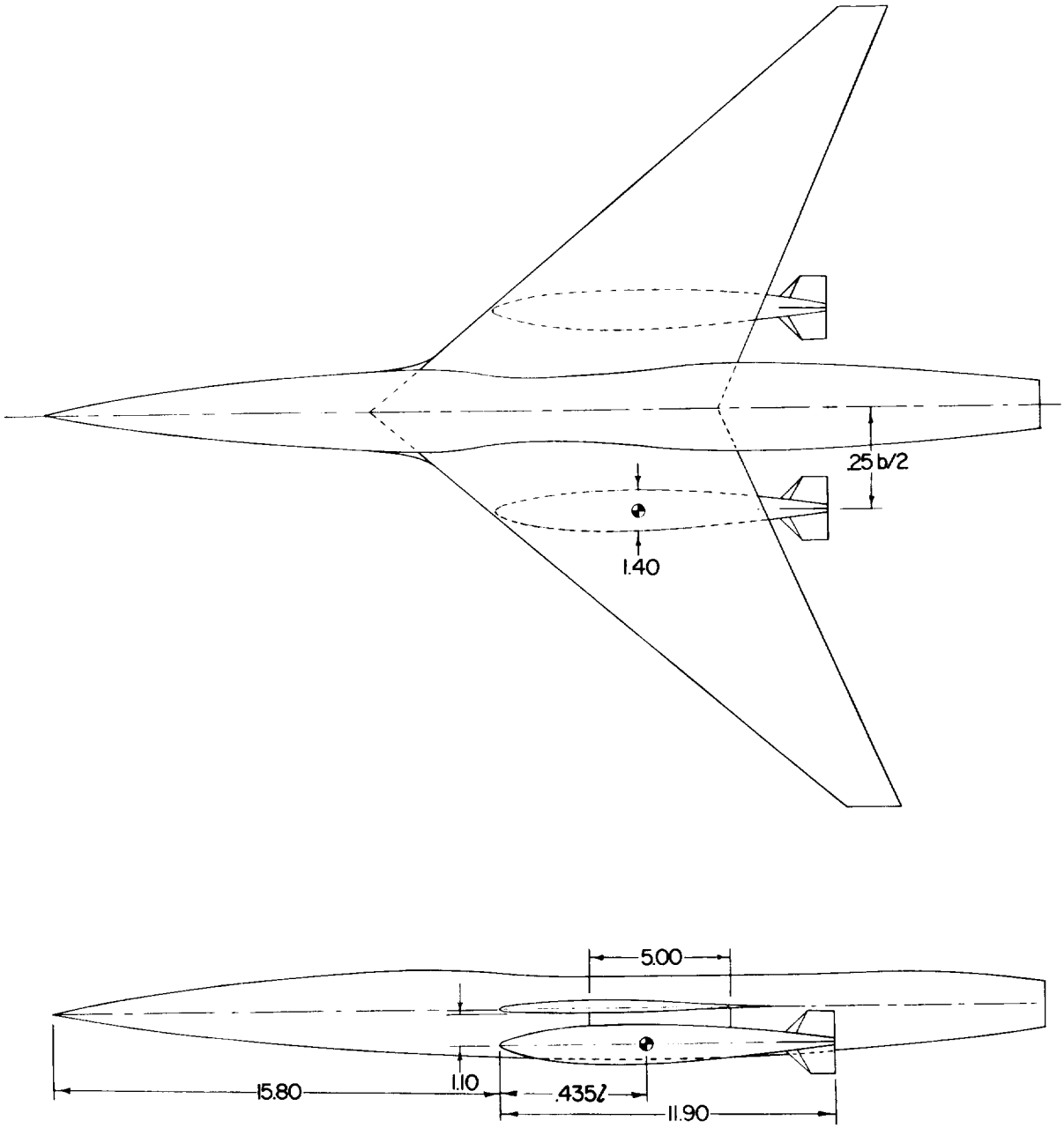

(b) Swept-wing—fuselage configuration with body pylon-mounted beneath the fuselage.

Figure 2.- Continued.

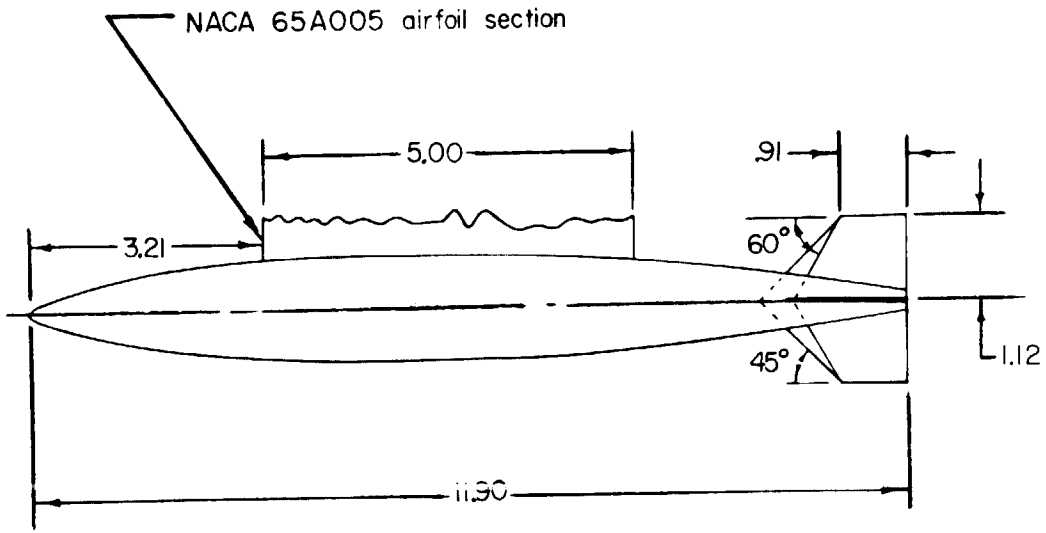

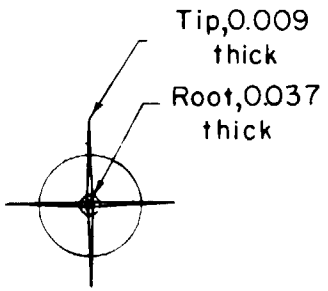

(c) Body and pylon.

Figure 2.- Concluded.

(a) Body pylon-mounted beneath the fuselage. L-93050

Figure 3.- Photographs of the model investigated installed in the Langley 8-foot transonic pressure tunnel.

(b) Bodies pylon-mounted beneath the wing. L-93090

Figure 3.- Concluded.

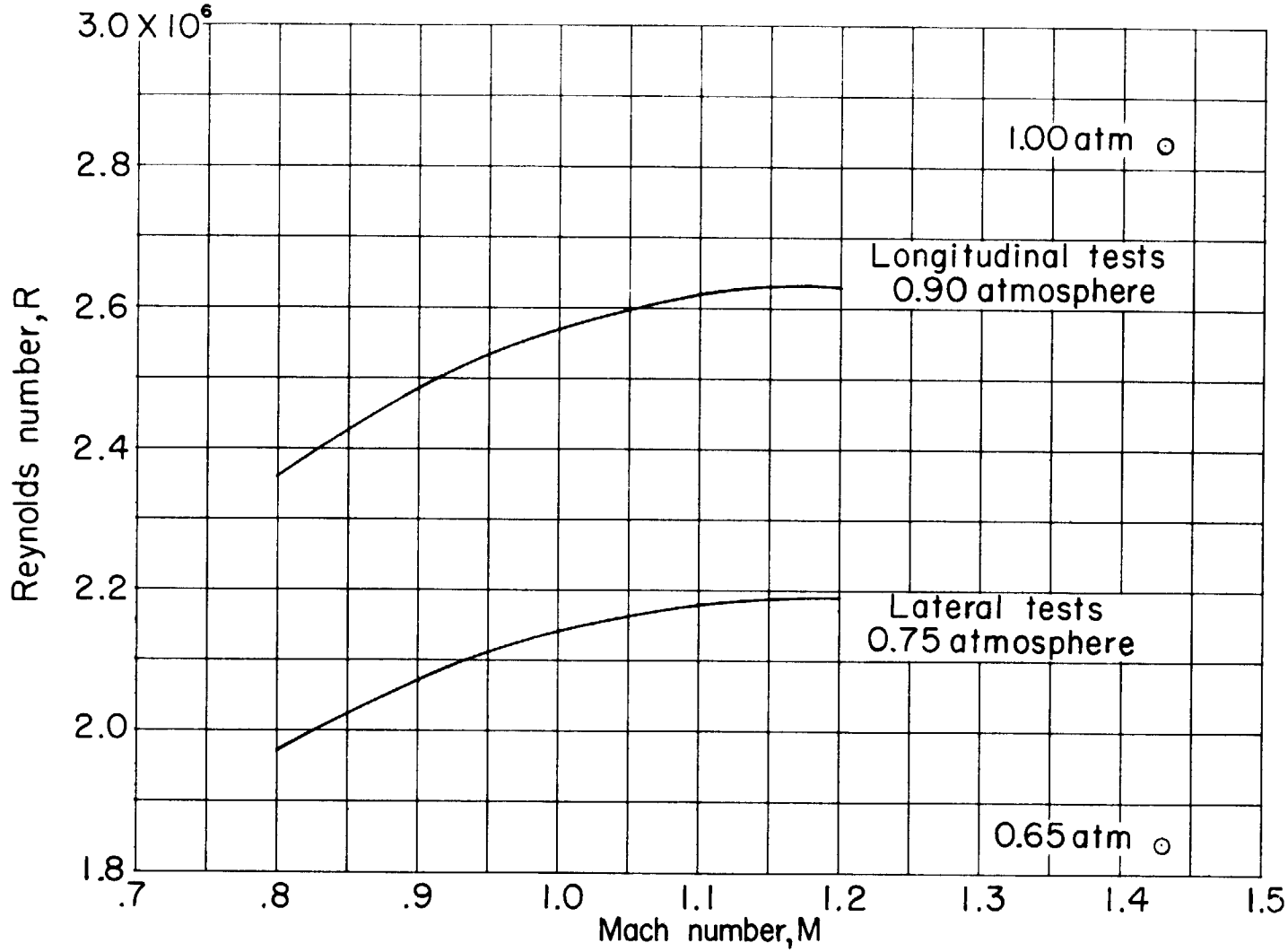

Figure 4.- Variation with Mach number of approximate test Reynolds number based on $\bar{c}$ = 8.421 inches.

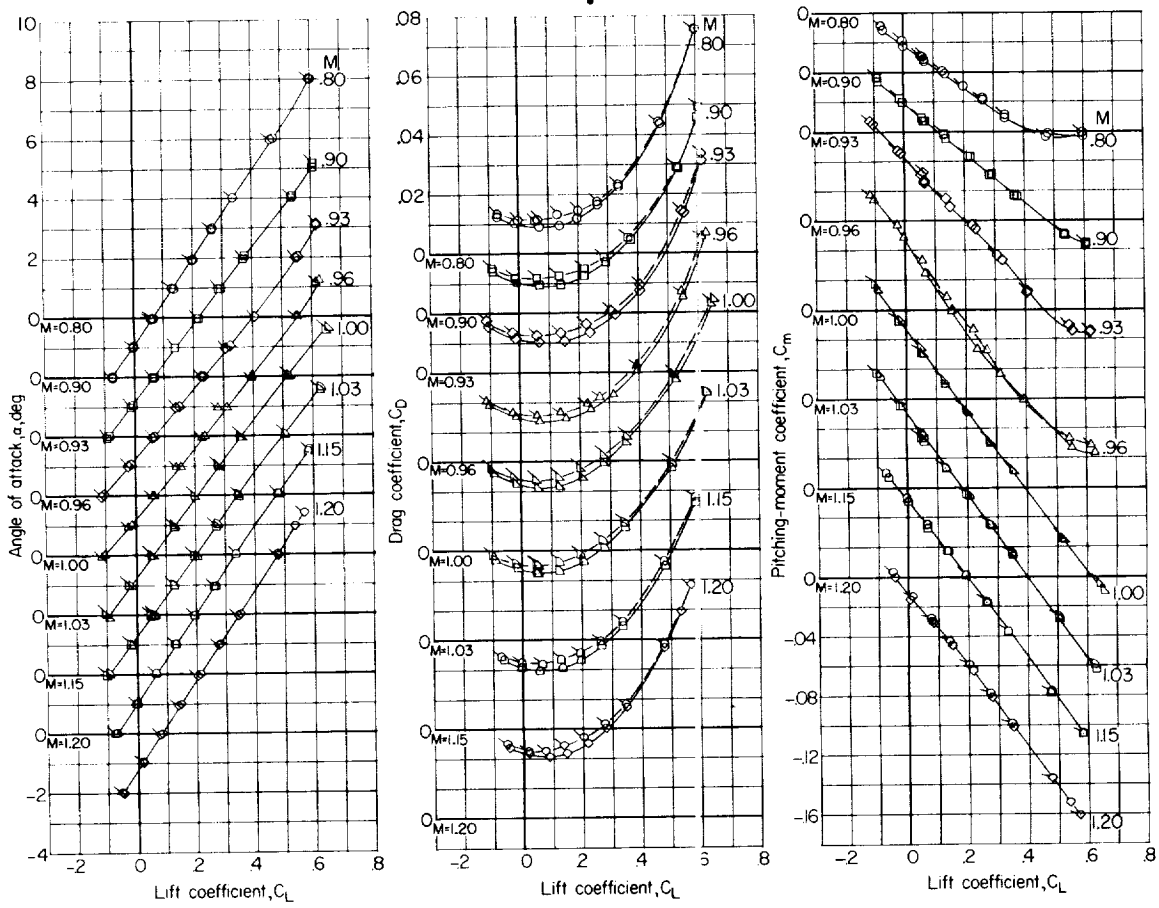

Figure 5.- Effects of transition on the longitudinal characteristics of the swept-wing—fuselage configuration with finned body pylon-mounted beneath the fuselage. Flagged symbols indicate fixed transition.

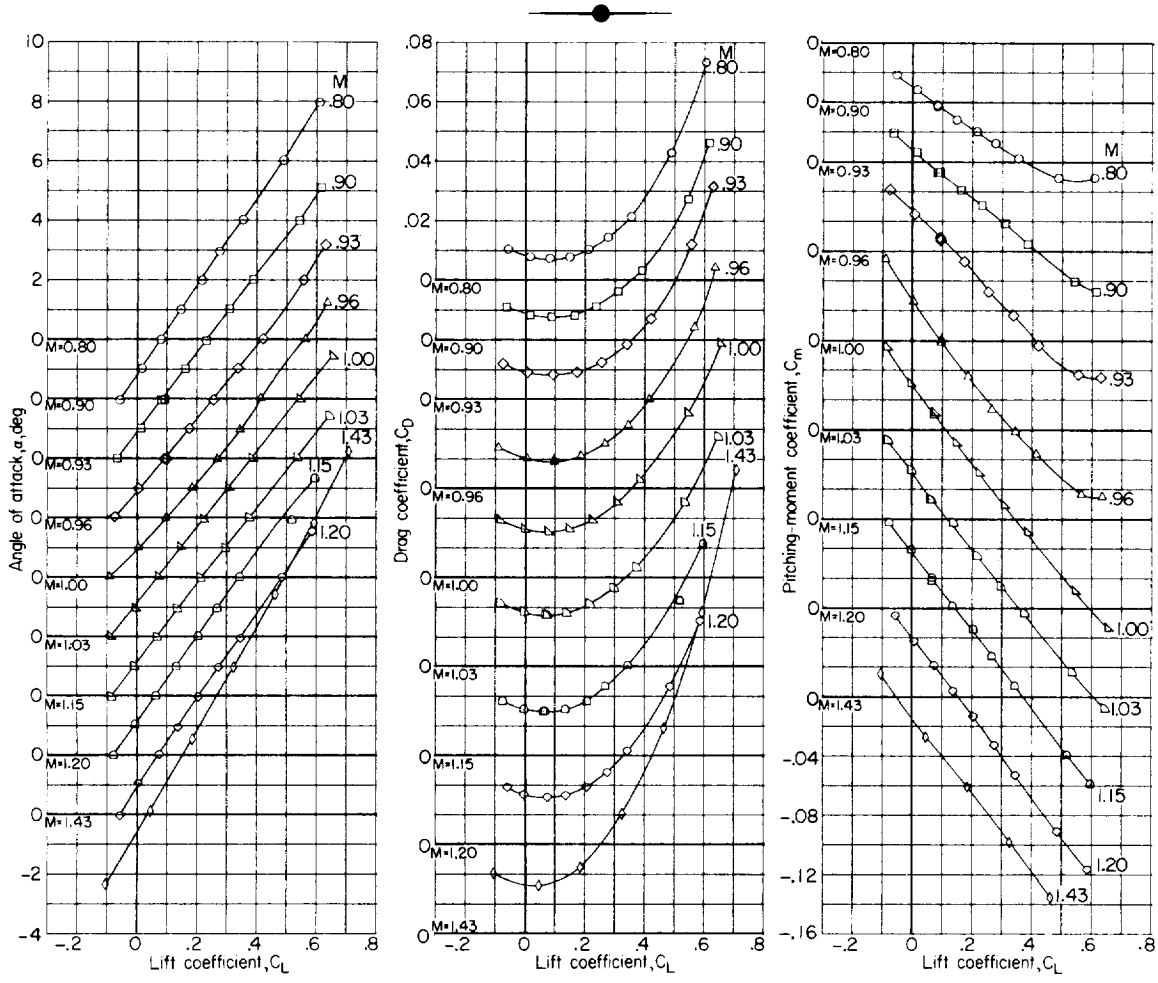

Figure 6.- Longitudinal characteristics of the swept-wing—fuselage configuration.

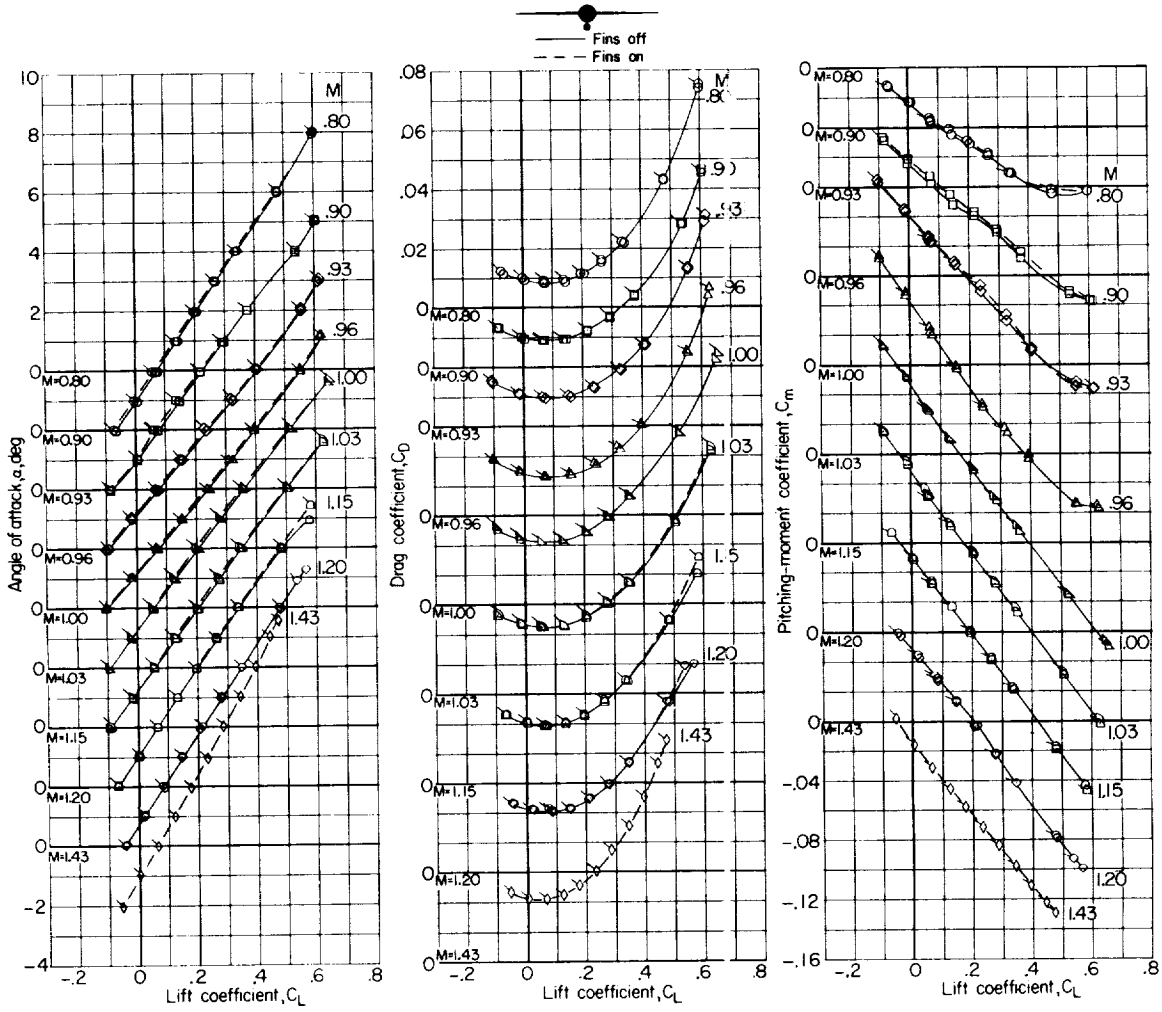

Figure 7.- Longitudinal characteristics of the swept-wing—fuselage configuration with finned and unfinned body pylon-mounted beneath the fuselage. Flagged symbols indicate fins on.

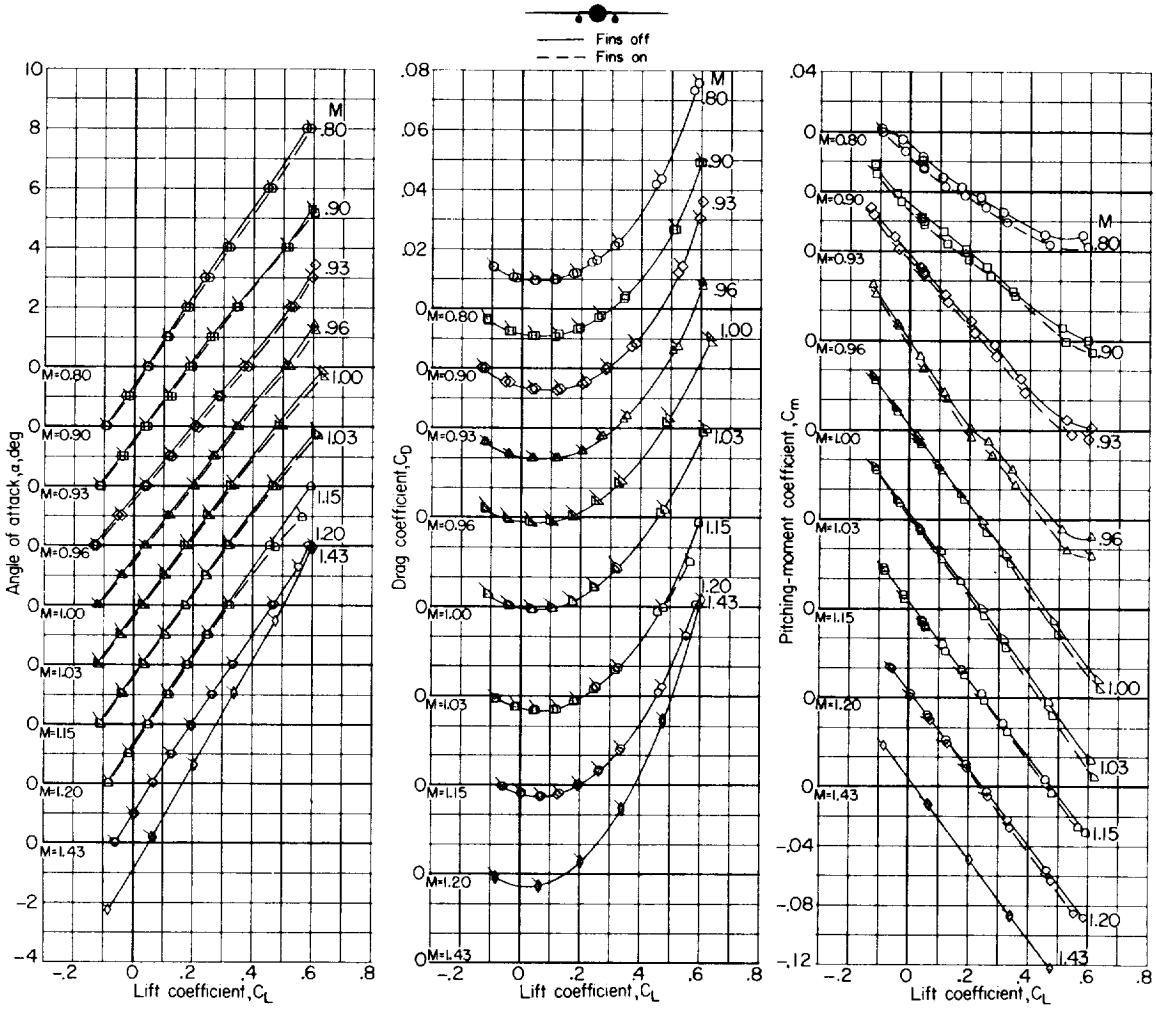

Figure 8.- Longitudinal characteristics of the swept-wing—fuselage configuration with finned and unfinned bodies pylon-mounted beneath the wing. Flagged symbols indicate fins on.

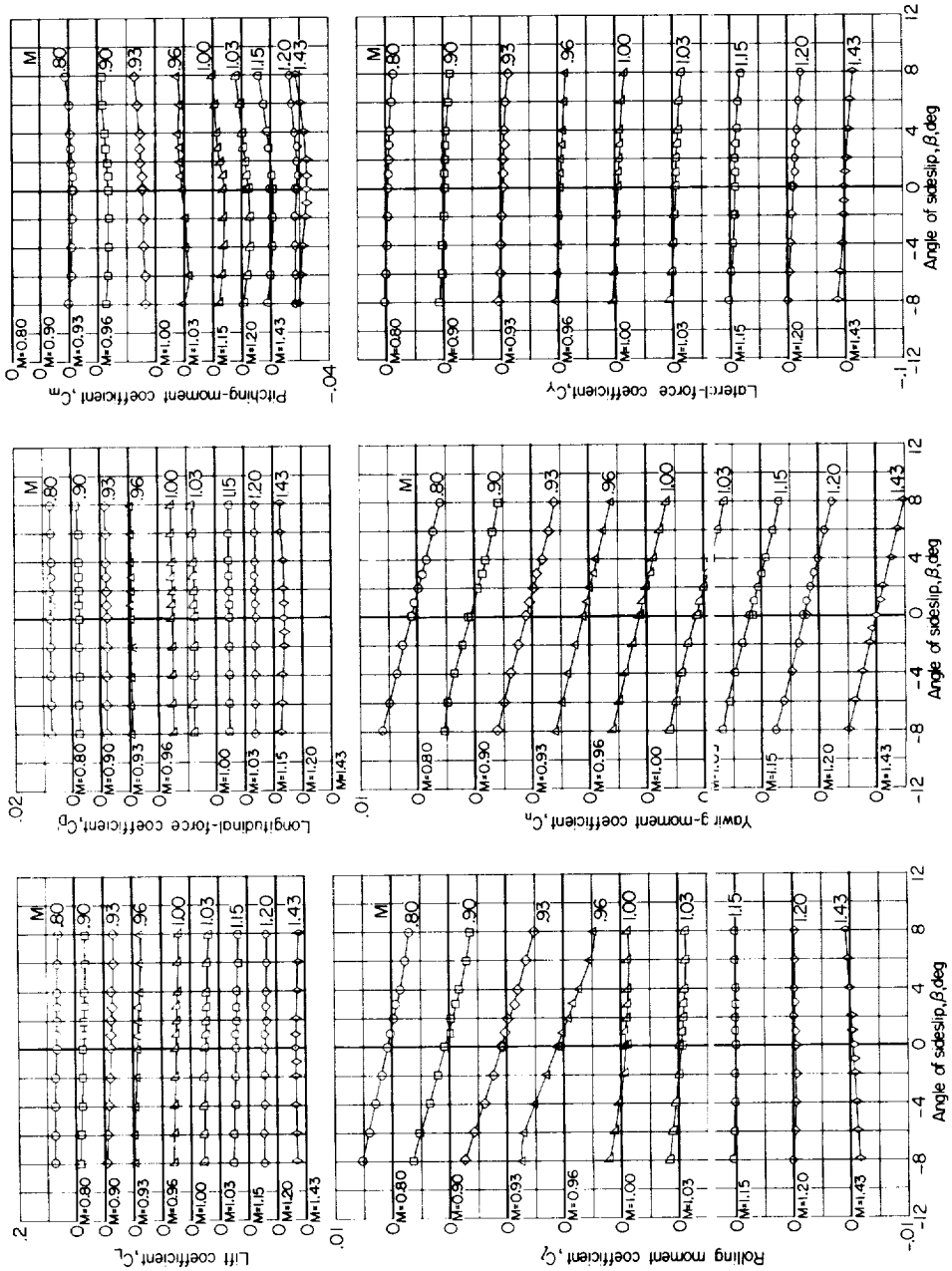

(a) $\alpha \approx -0.2^{\circ}$.

Figure 9.- Variation with angle of sideslip of the aerodynamic characteristics of the swept-wing—fuselage configuration.

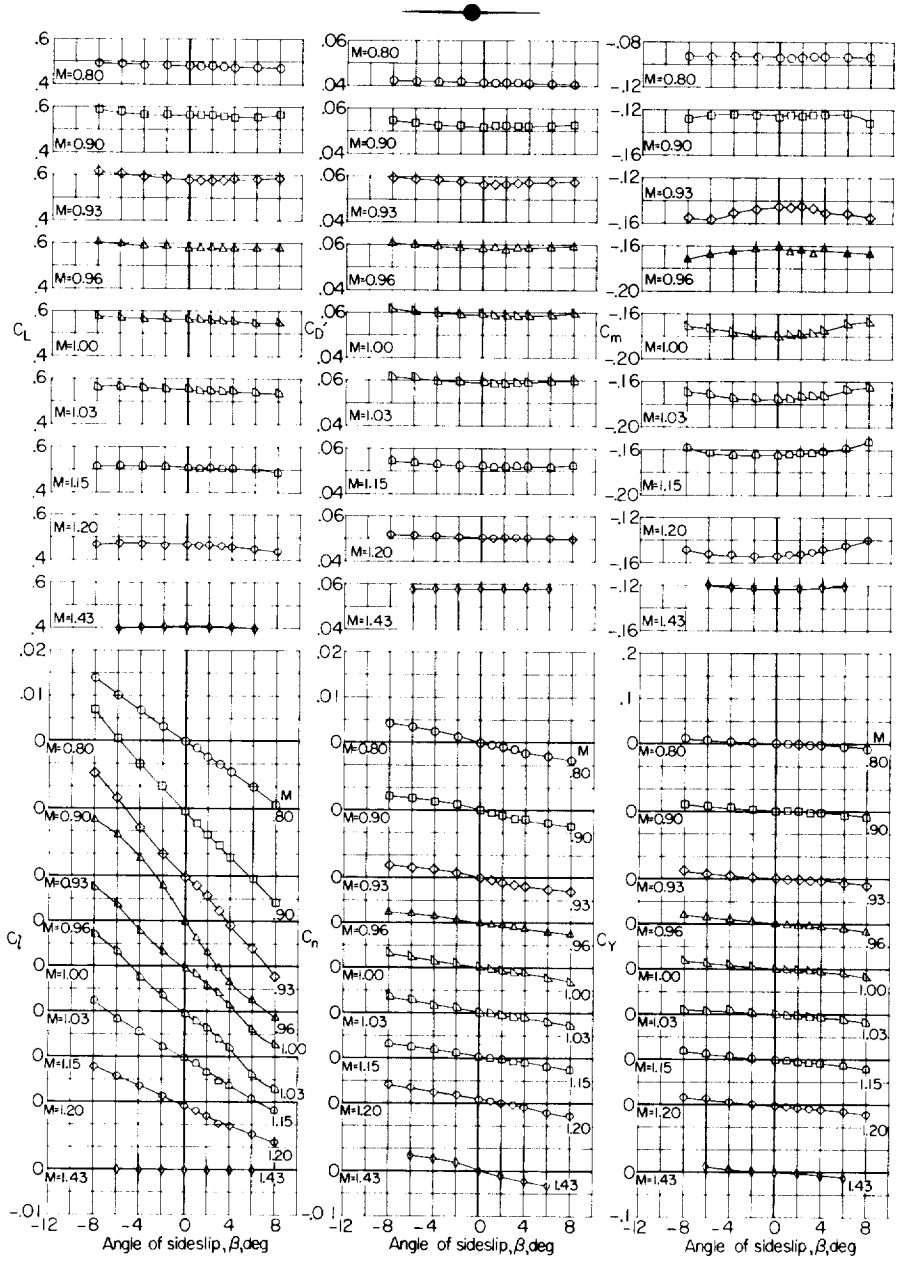

(b) $\alpha \approx 5.9^{\circ}$.

Figure 9.- Concluded.

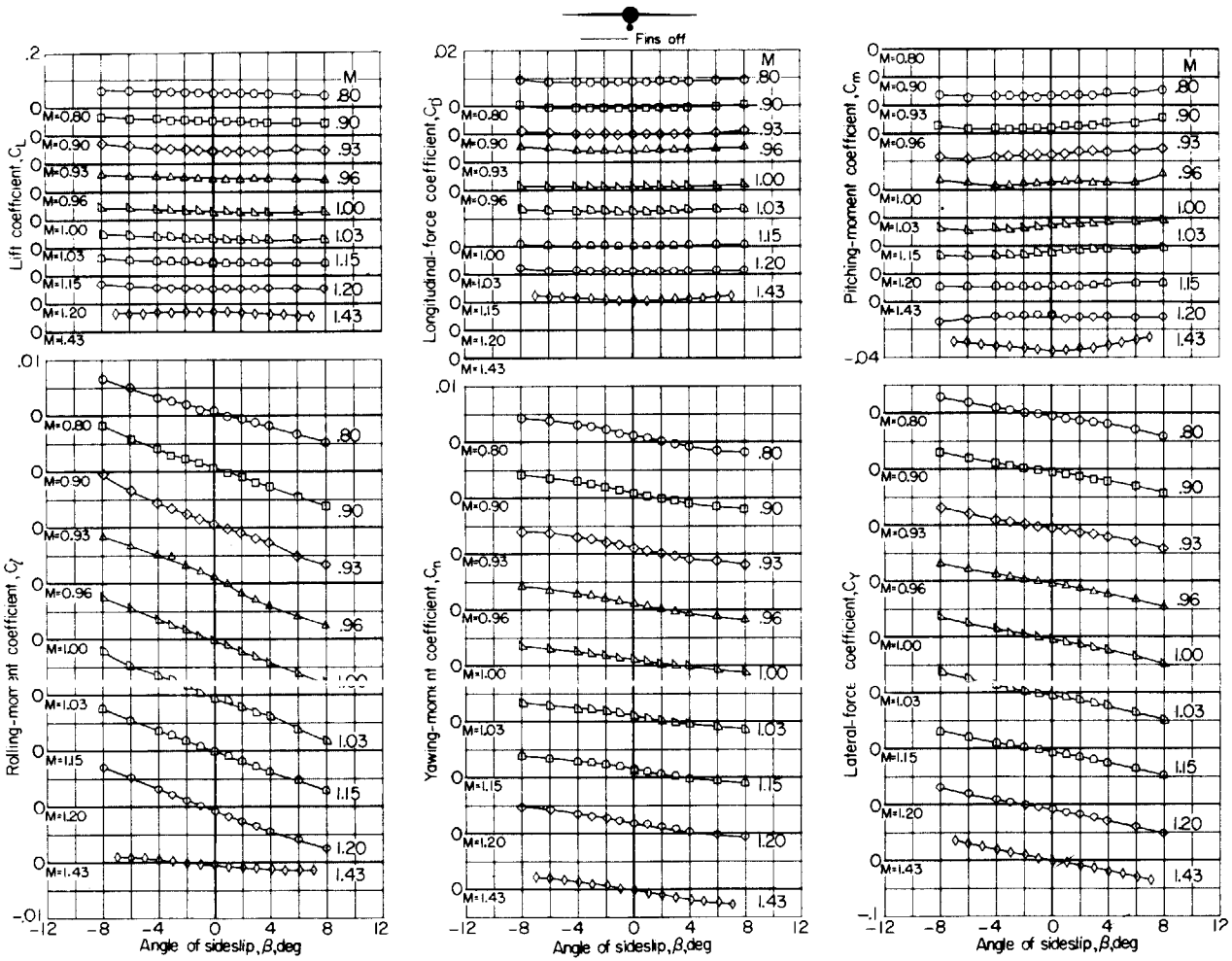

(a) $\alpha \approx -0.2^{\circ}$.

Figure 10.- Variation with angle of sideslip of the aerodynamic characteristics of the swept-wing—fuselage configuration with finned and unfinned body pylon-mounted beneath the fuselage.

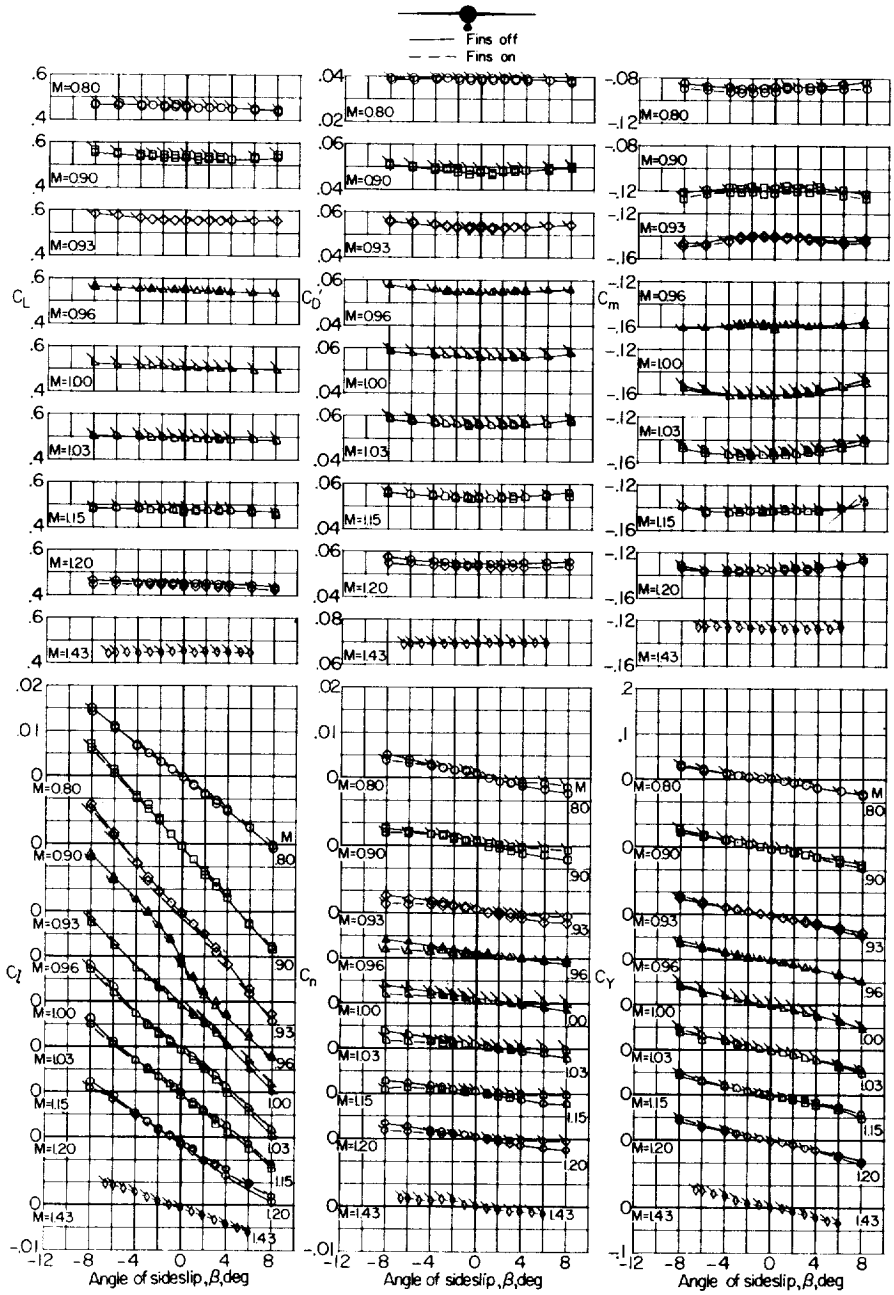

(b) $\alpha \approx 5.7^{\circ}$.

Figure 10.- Concluded.

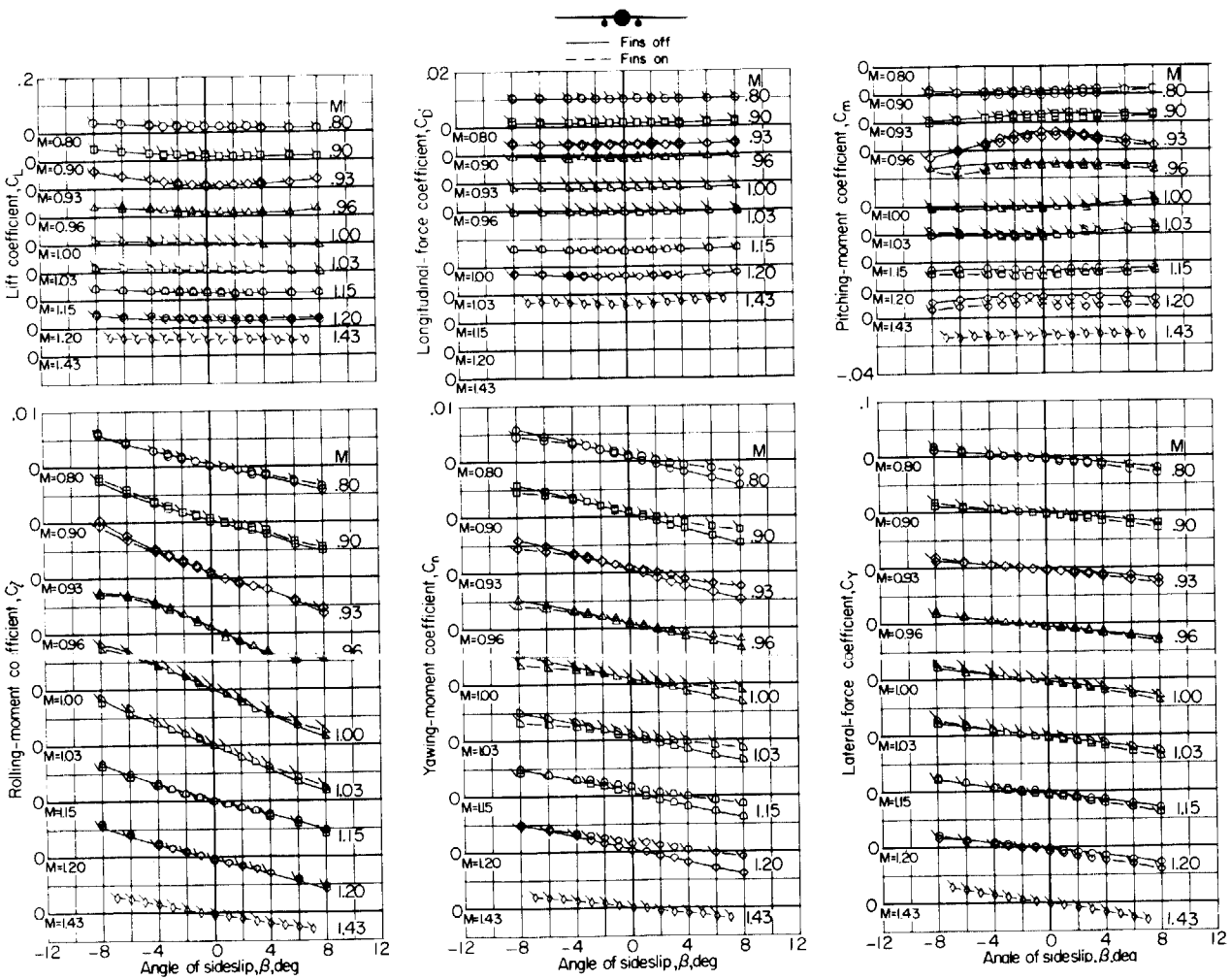

(a) $\alpha \approx -0.2^{\circ}$.

Figure 11.- Variation with angle of sideslip of the aerodynamic characteristics of the swept-wing—fuselage configuration with finned and unfinned bodies pylon-mounted beneath the wing. Flagged symbols indicate fins on.

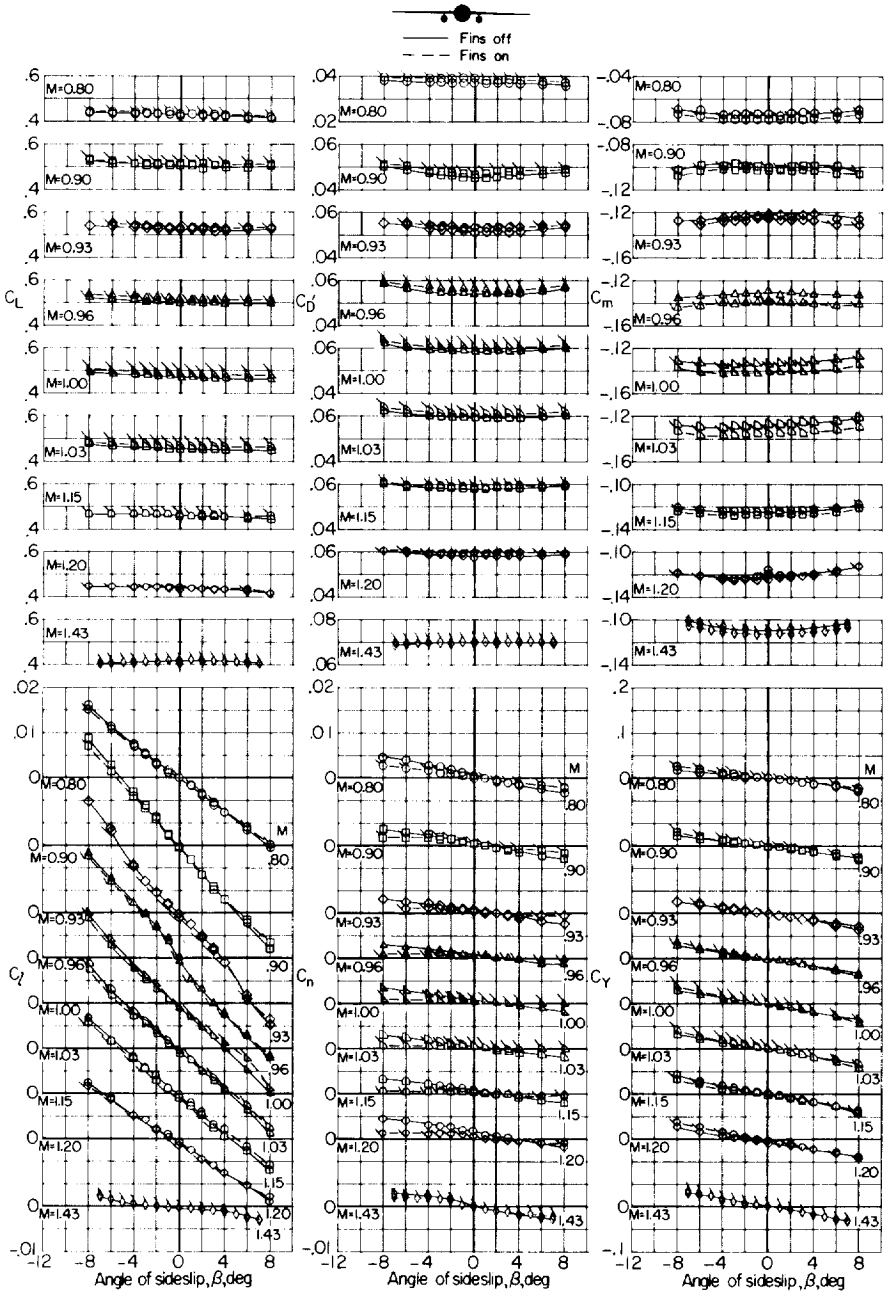

(b) $\alpha \approx 5.6^{\circ}$.

Figure 11.- Concluded.

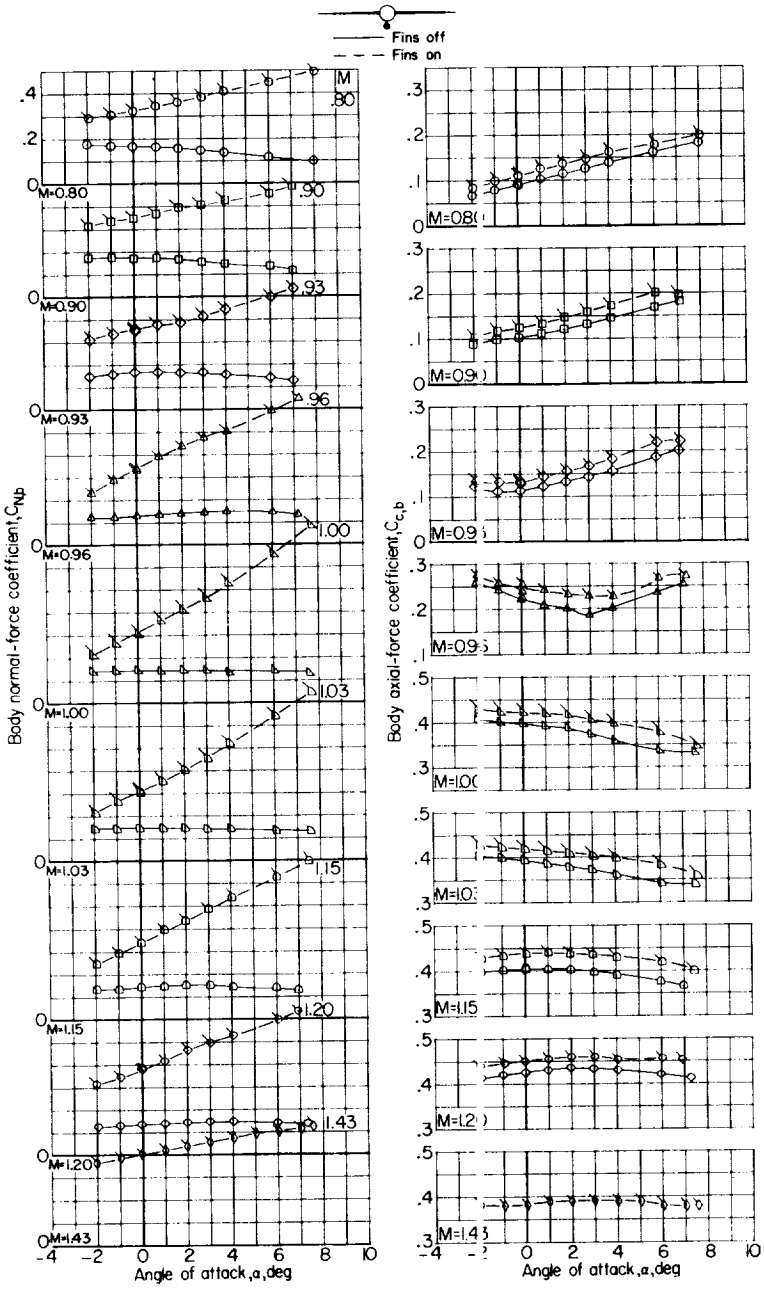

Figure 12.- Variation with angle of attack of loads on the finned and unfinned body pylon-mounted beneath the fuselage. Flagged symbols indicate fins on.

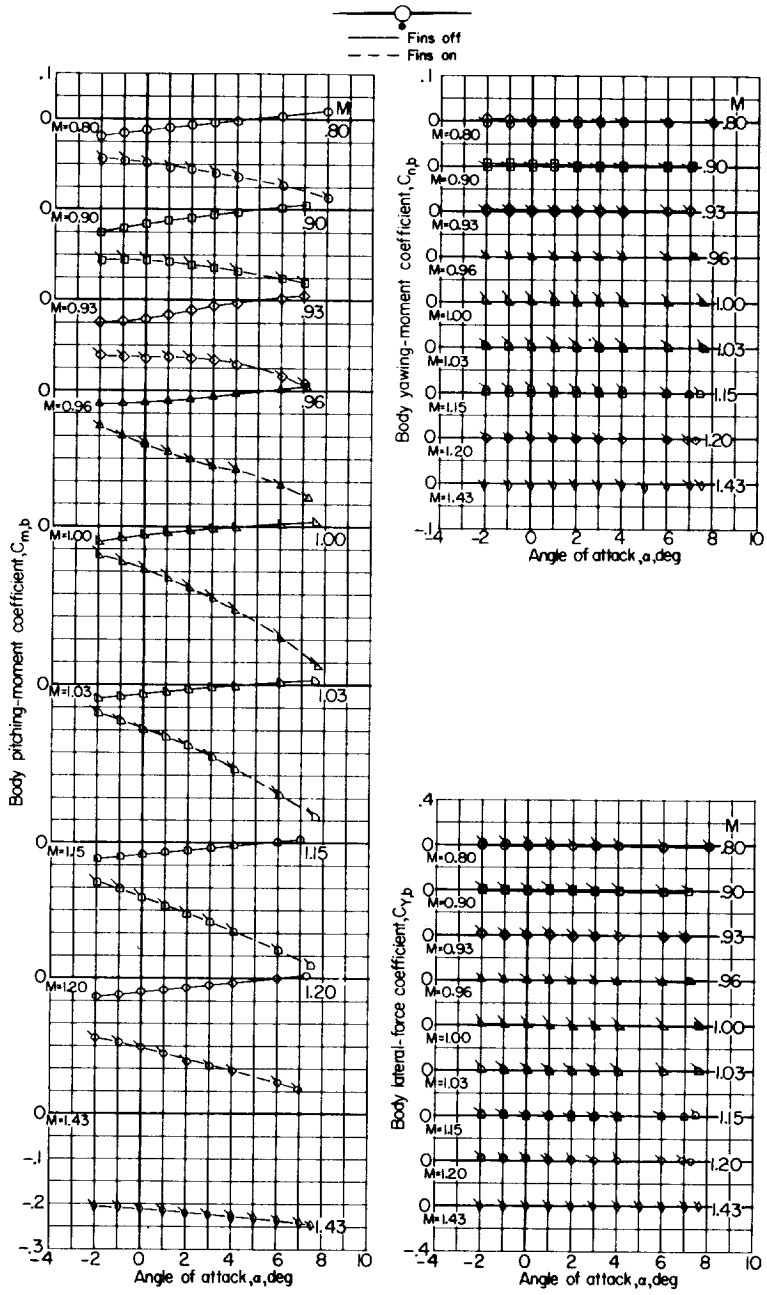

Figure 12.- Concluded.

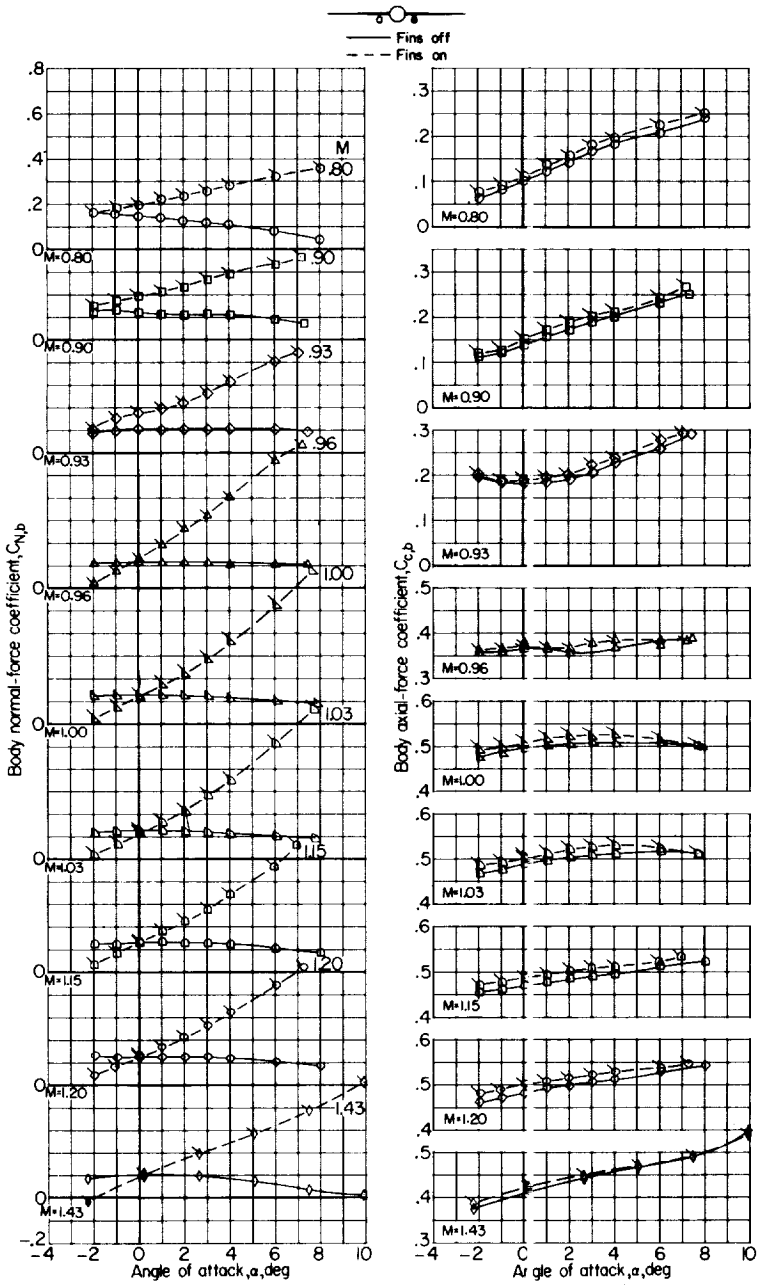

Figure 13.- Variation with angle of attack of loads on the finned and unfinned body pylon-mounted beneath the left wing. Flagged symbols indicate fins on.

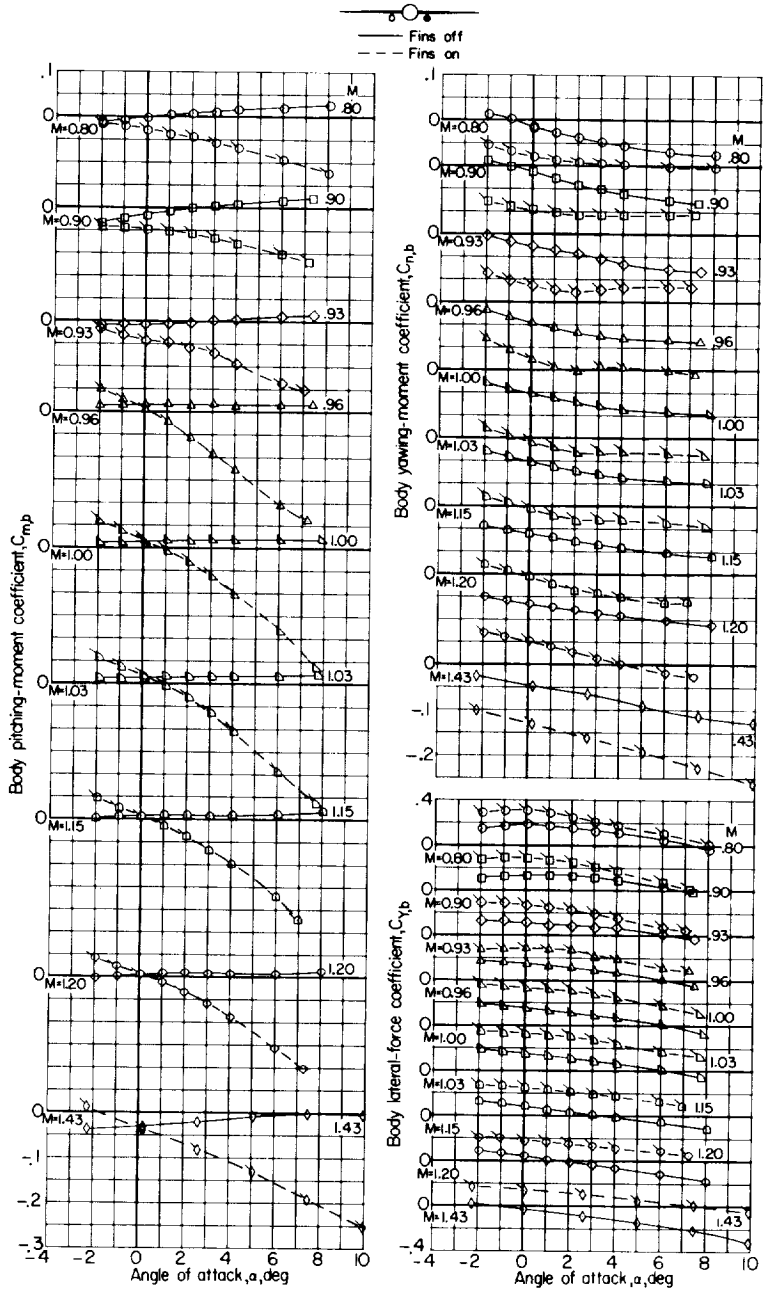

Figure 13.- Concluded.

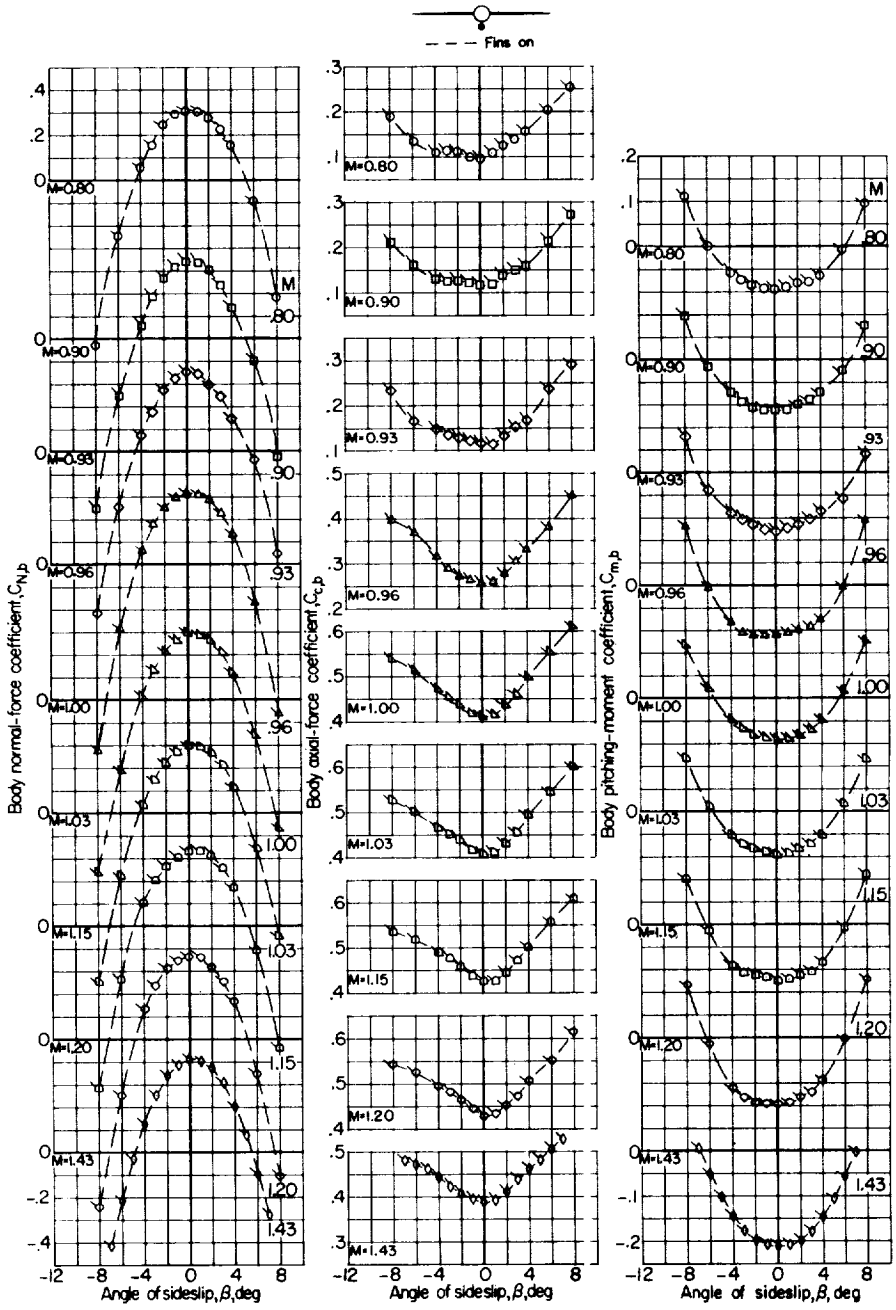

(a) $\alpha \approx -0.2^{\circ}$.

Figure 14.- Variation with angle of sideslip of loads on the finned and unfinned body pylon-mounted beneath the fuselage. Flagged symbols indicate fins on.

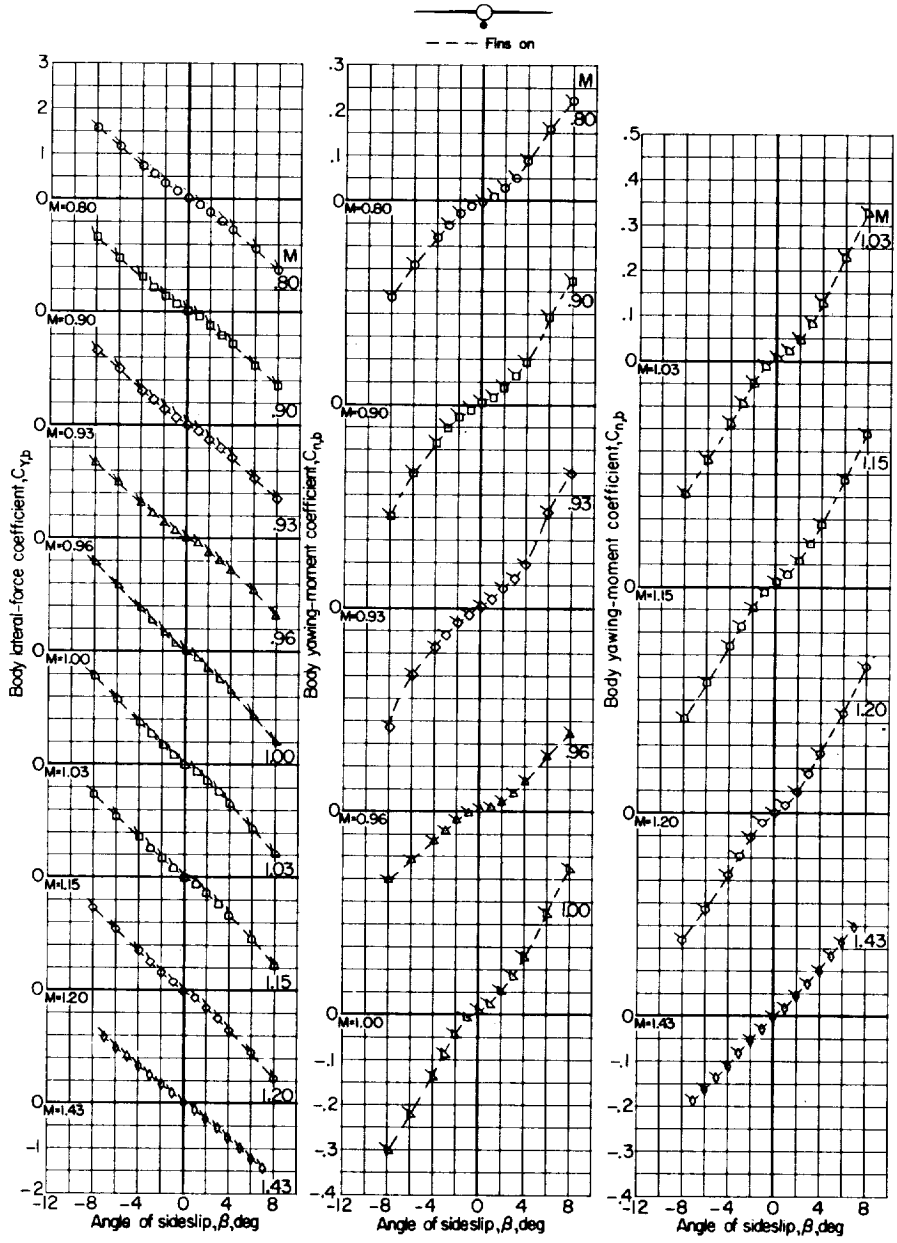

(a) $\alpha \approx -0.2^{\circ}$. Concluded.

Figure 14.- Continued.

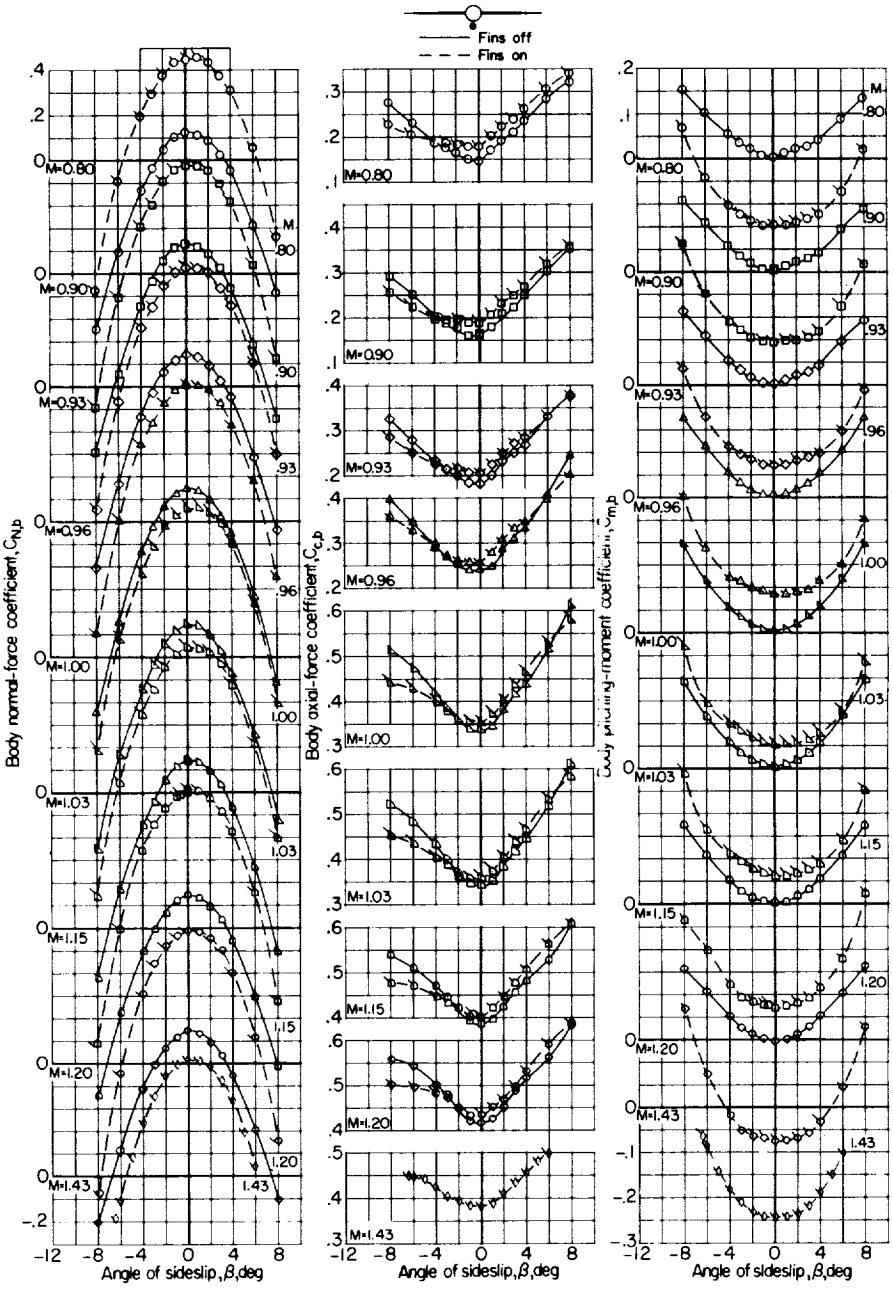

(b) $\alpha \approx 5.7^{\circ}$.

Figure 14.- Continued.

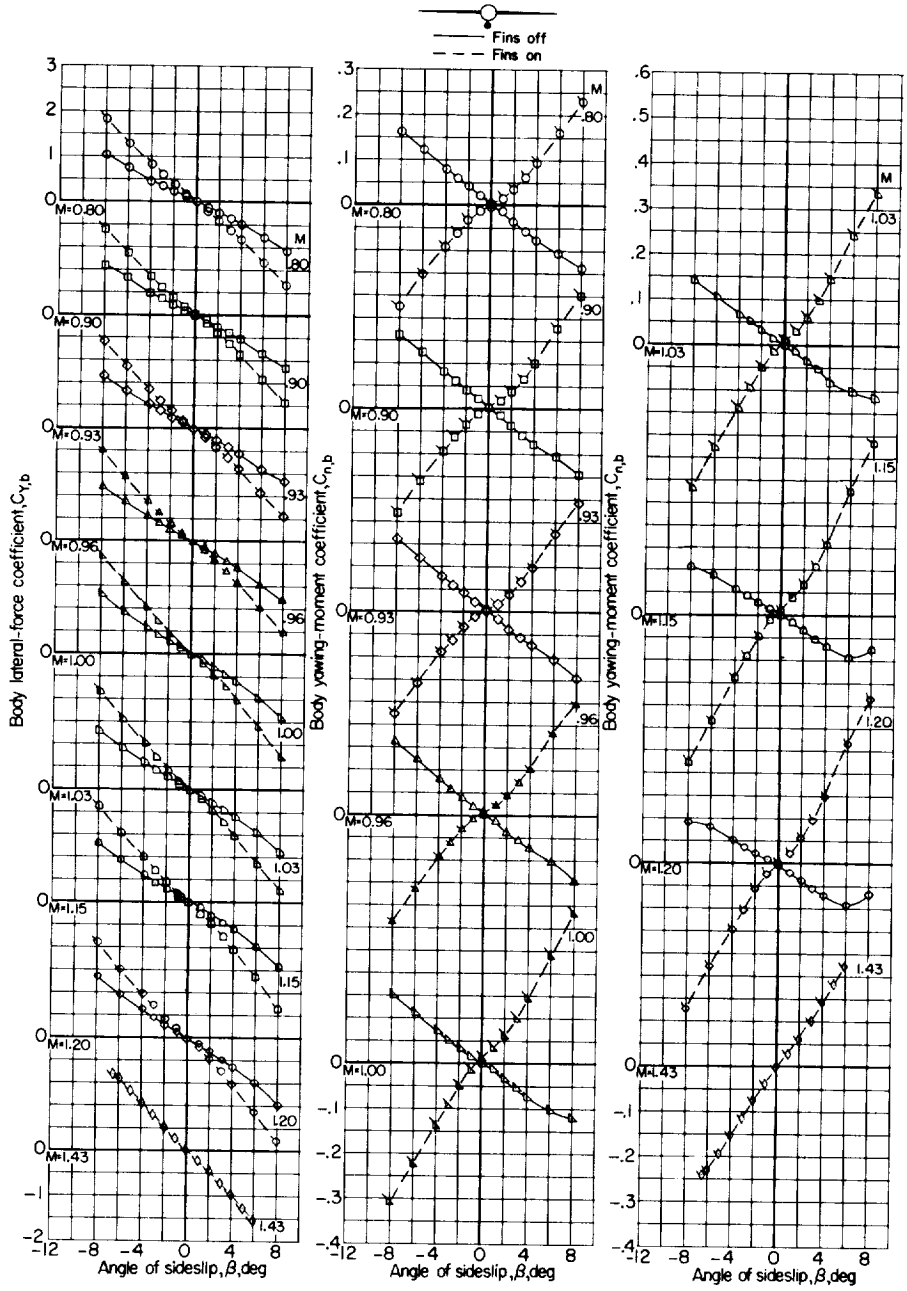

(b) $\alpha \approx 5.7^{\circ}$. Concluded.

Figure 14.- Concluded.

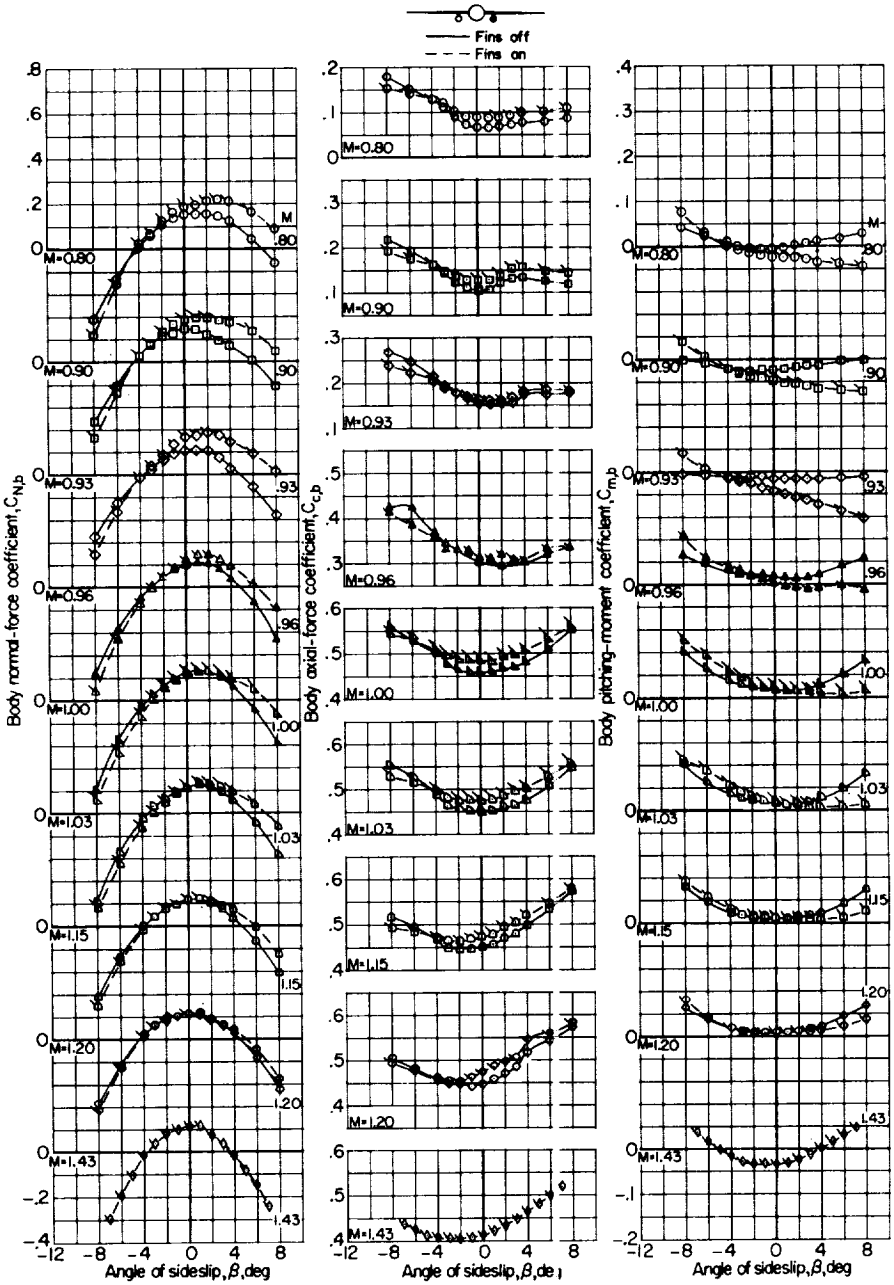

(a) $\alpha \approx -0.2^{\circ}$.

Figure 15.- Variation with angle of sideslip of loads on the finned and unfinned body pylon-mounted beneath the left wing. Flagged symbols indicate fins on.

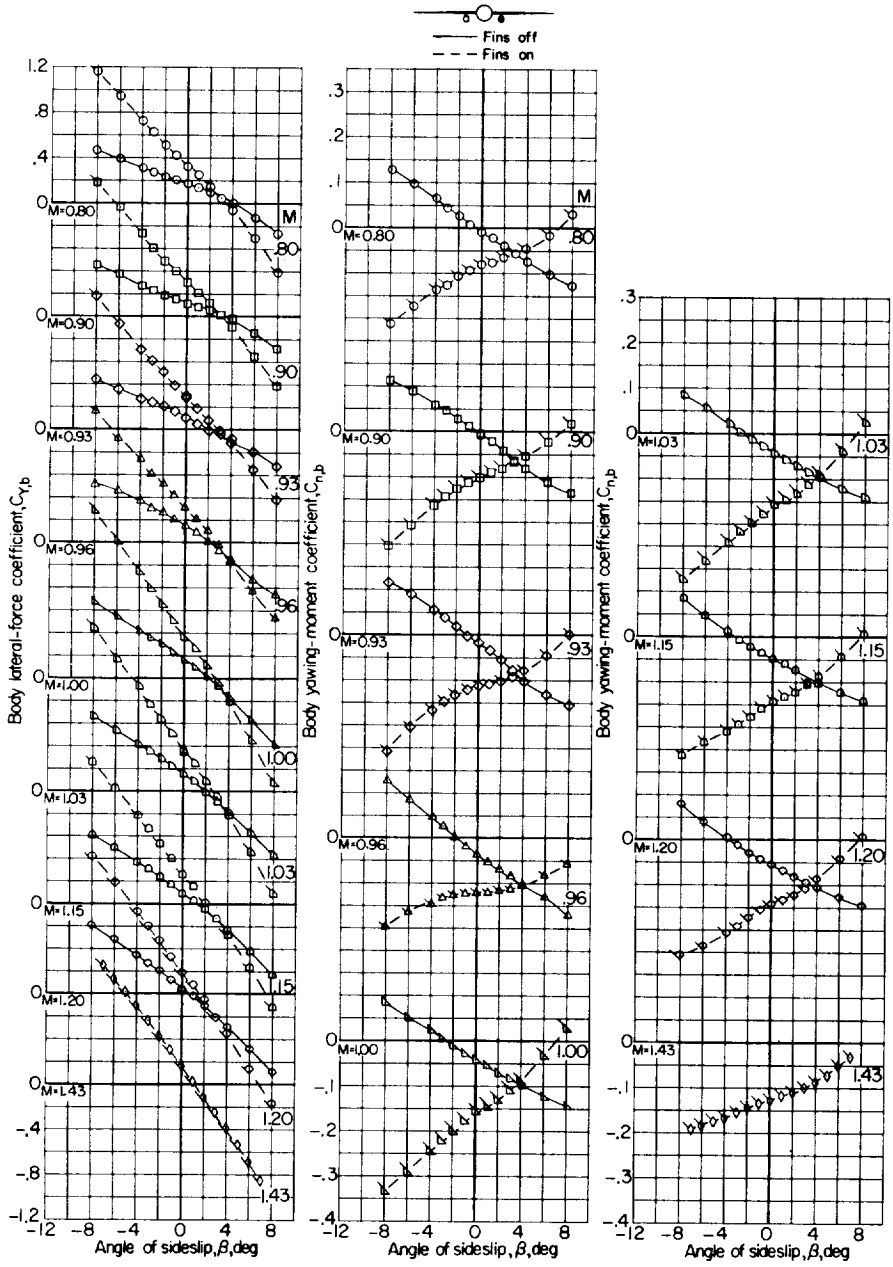

(a) $\alpha \approx -0.2^{\circ}$. Concluded.

Figure 15.- Continued.

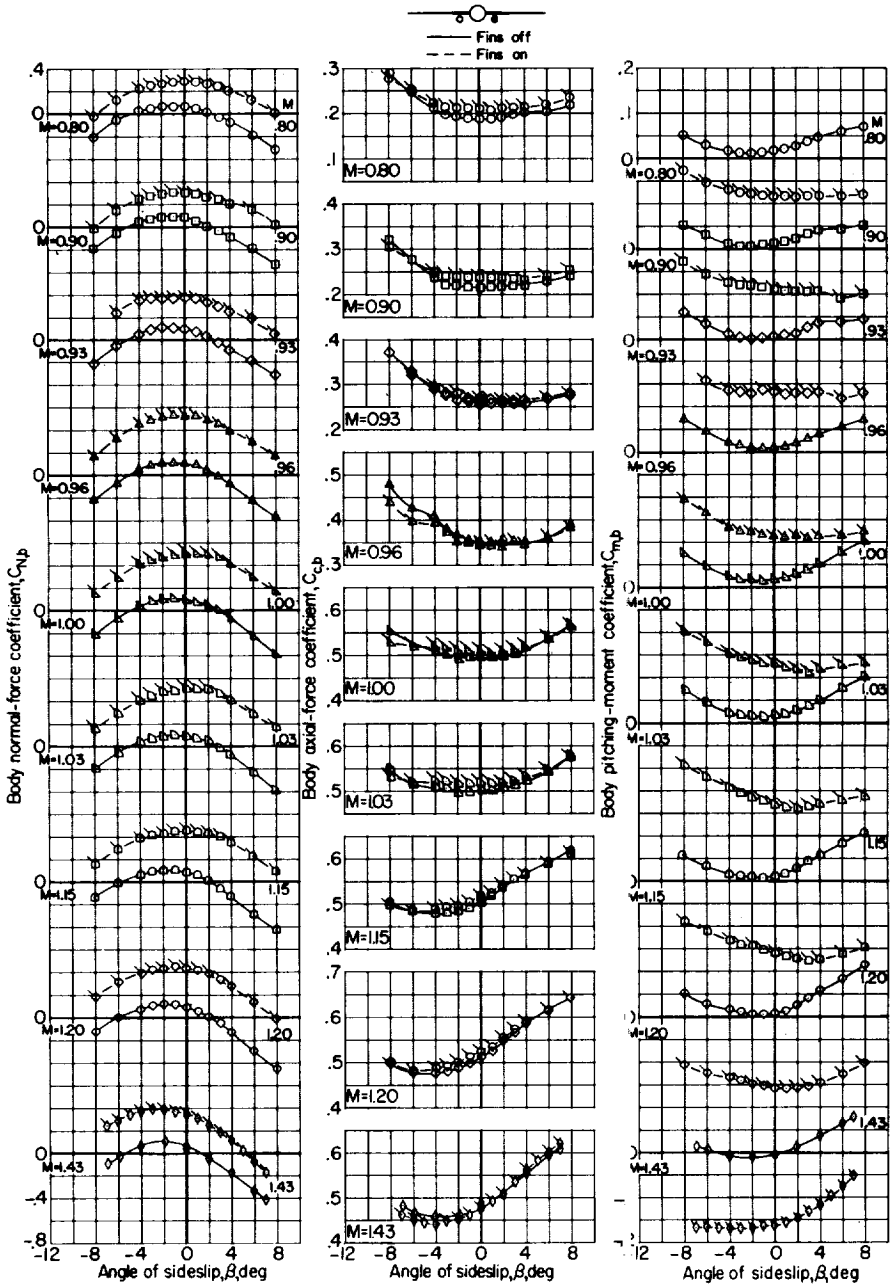

(b) $\alpha \approx 5.6^{\circ}$.

Figure 15.- Continued.

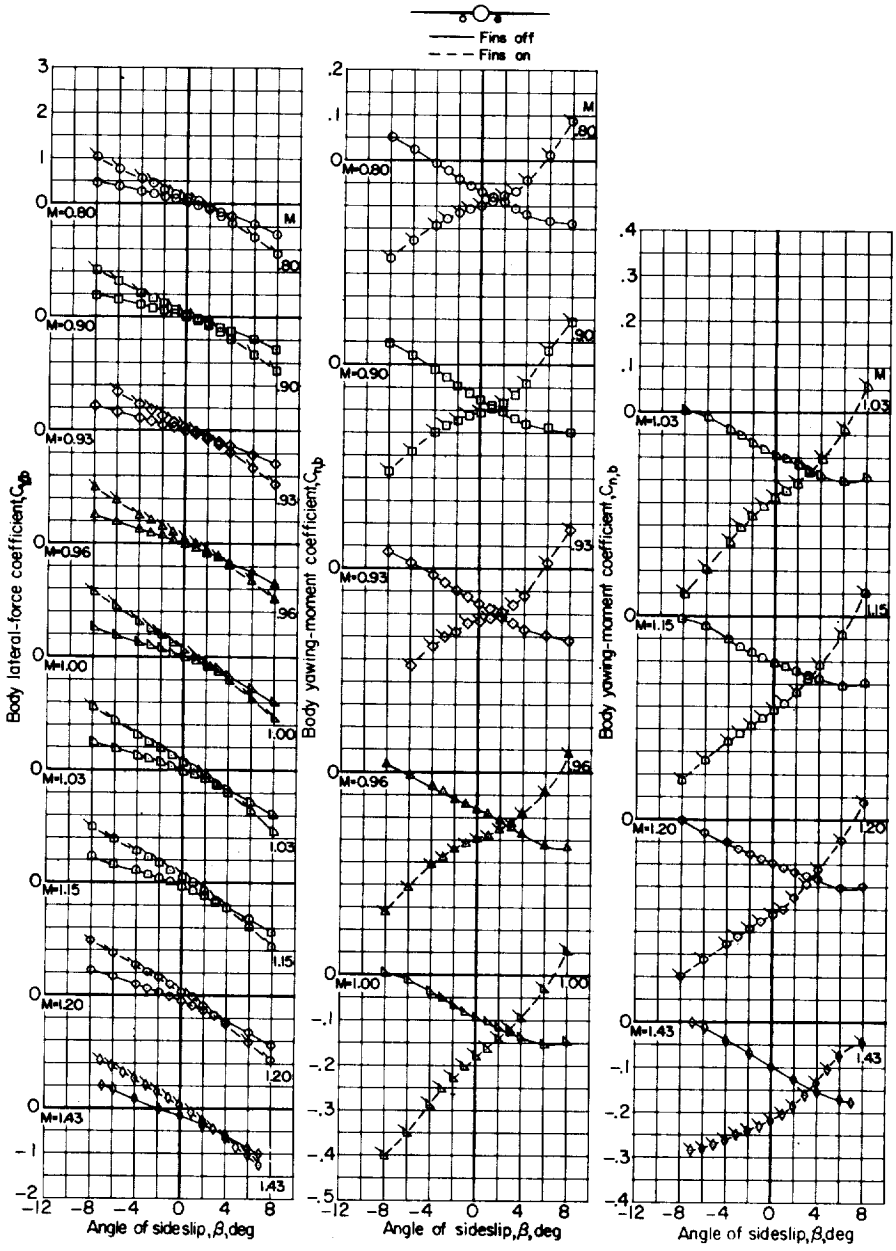

(b) $\alpha \approx 5.6^{\circ}$. Concluded.

Figure 15.- Concluded.

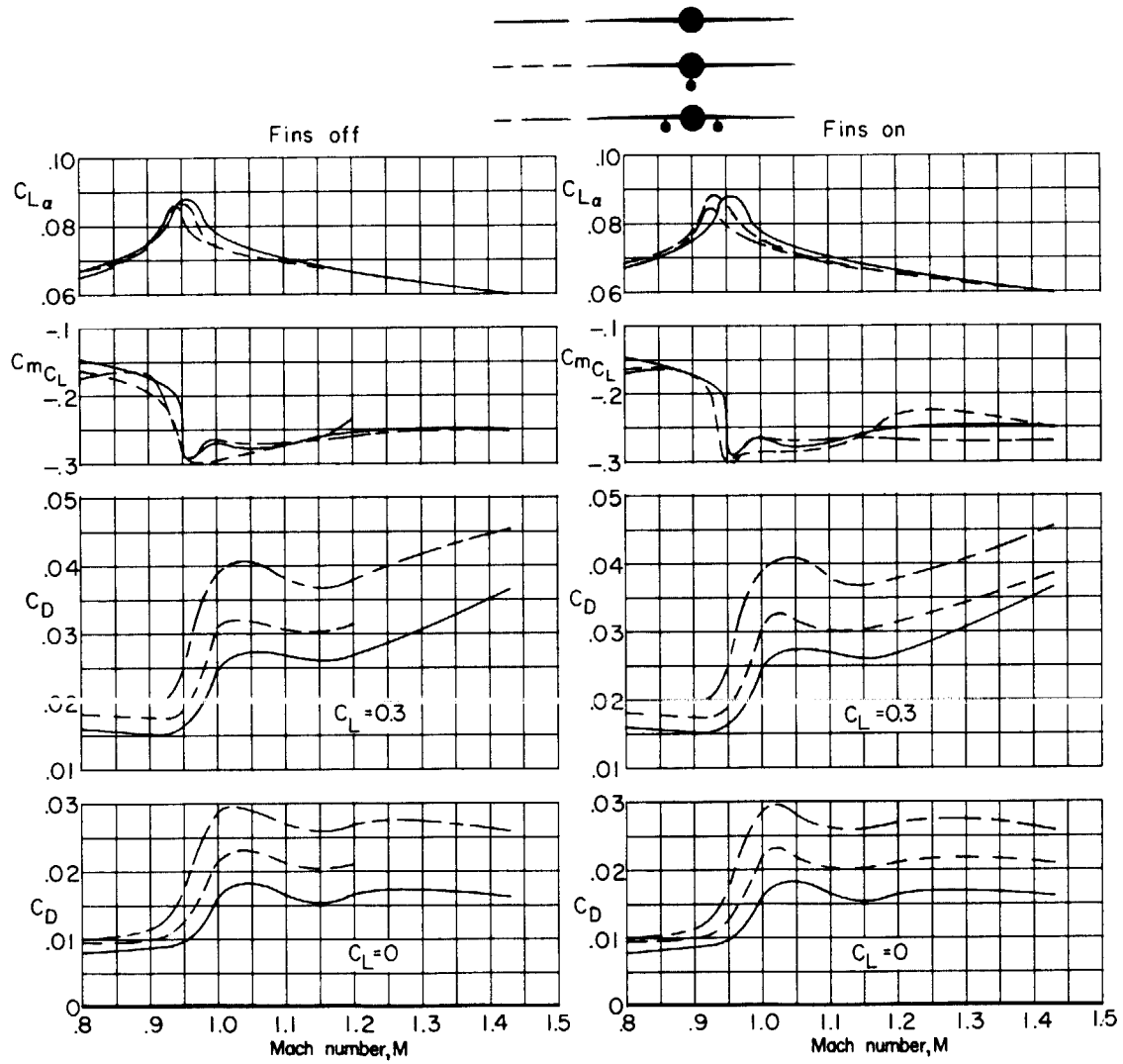

Figure 16.- Variation with Mach number of the longitudinal characteristics of the swept-wing—fuselage configuration with and without bodies.

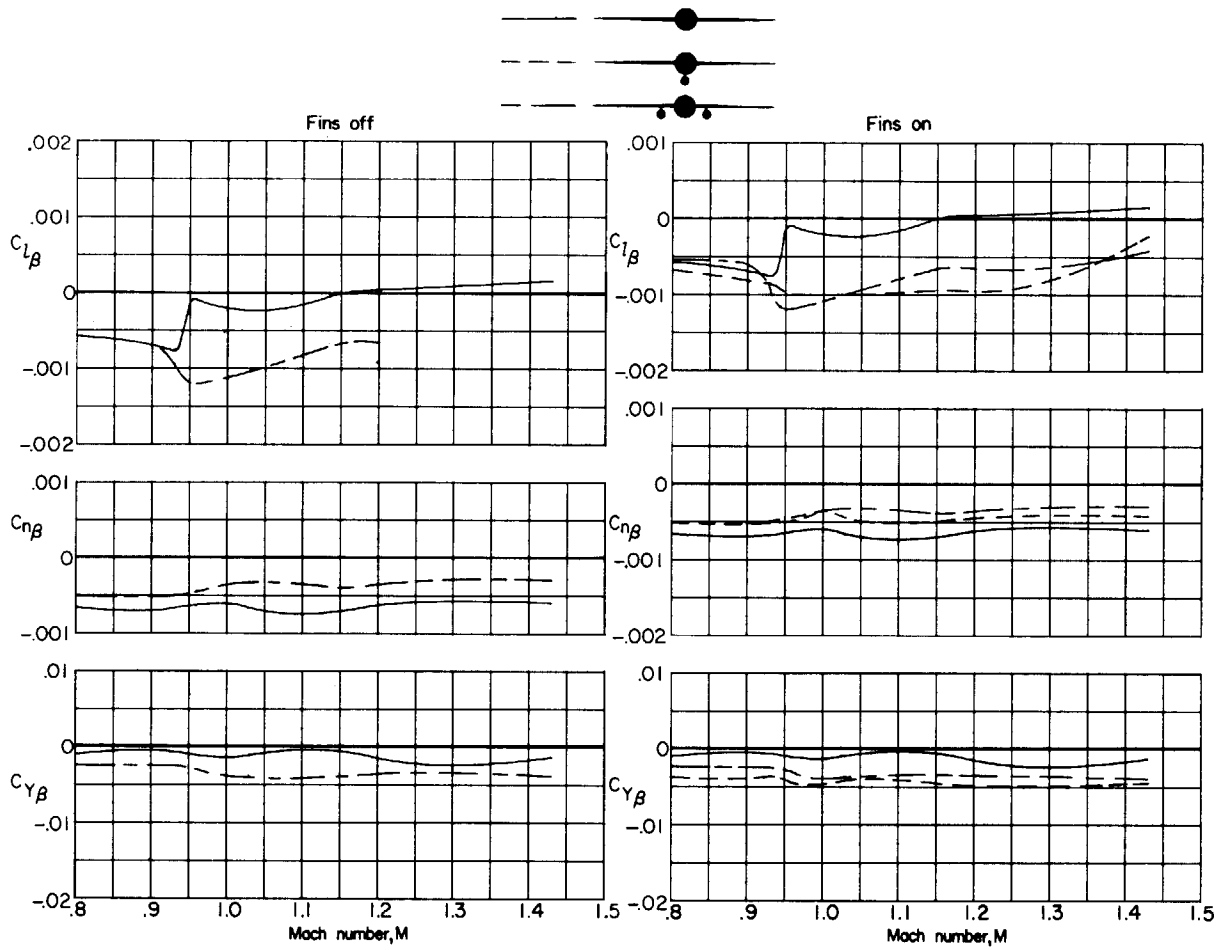

(a) $\alpha \approx -0.2^{\circ}$.

Figure 17.- Variation with Mach number of the lateral characteristics of the swept-wing—fuselage configuration with and without bodies.

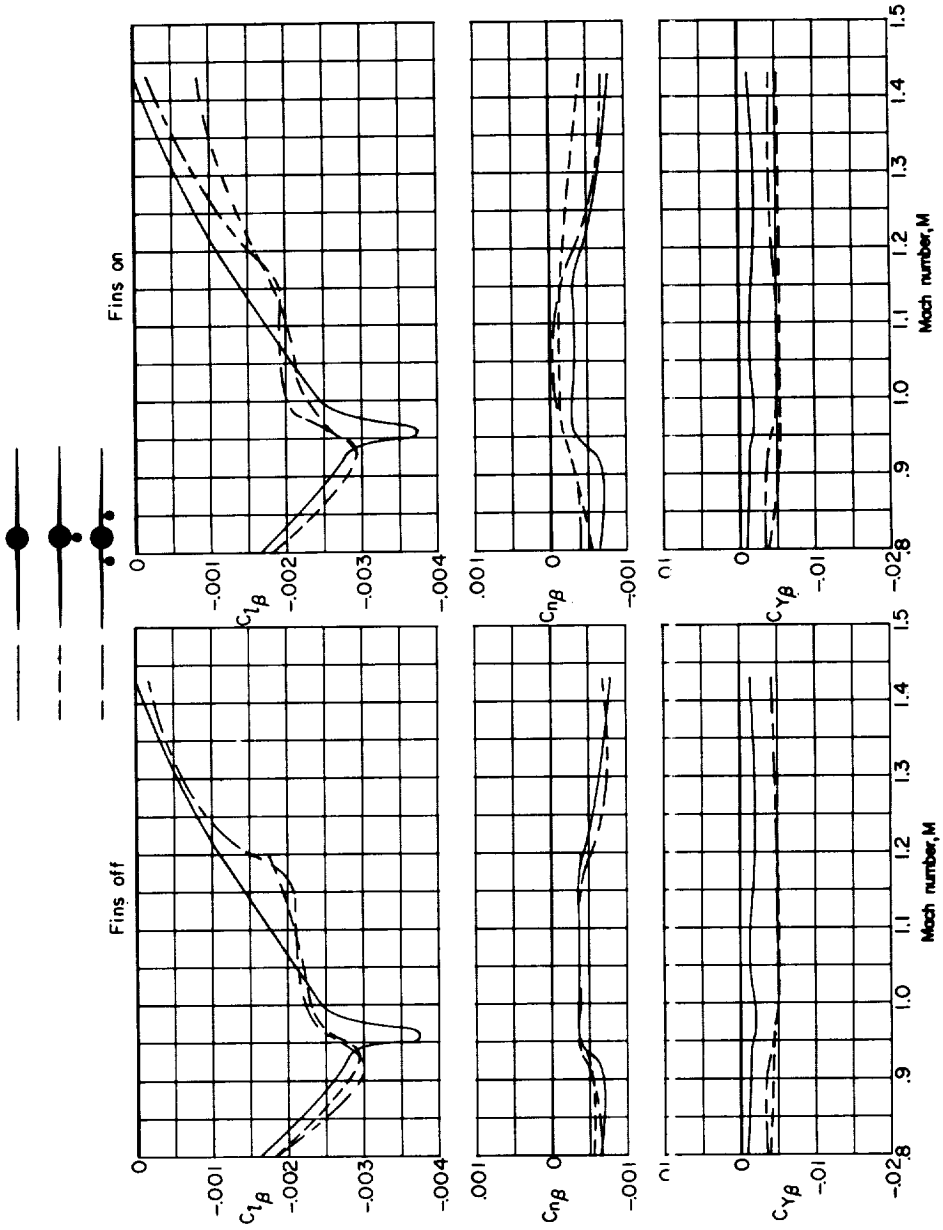

(b) $\alpha \approx 5.7^{\circ}$.

Figure 17.- Concluded.

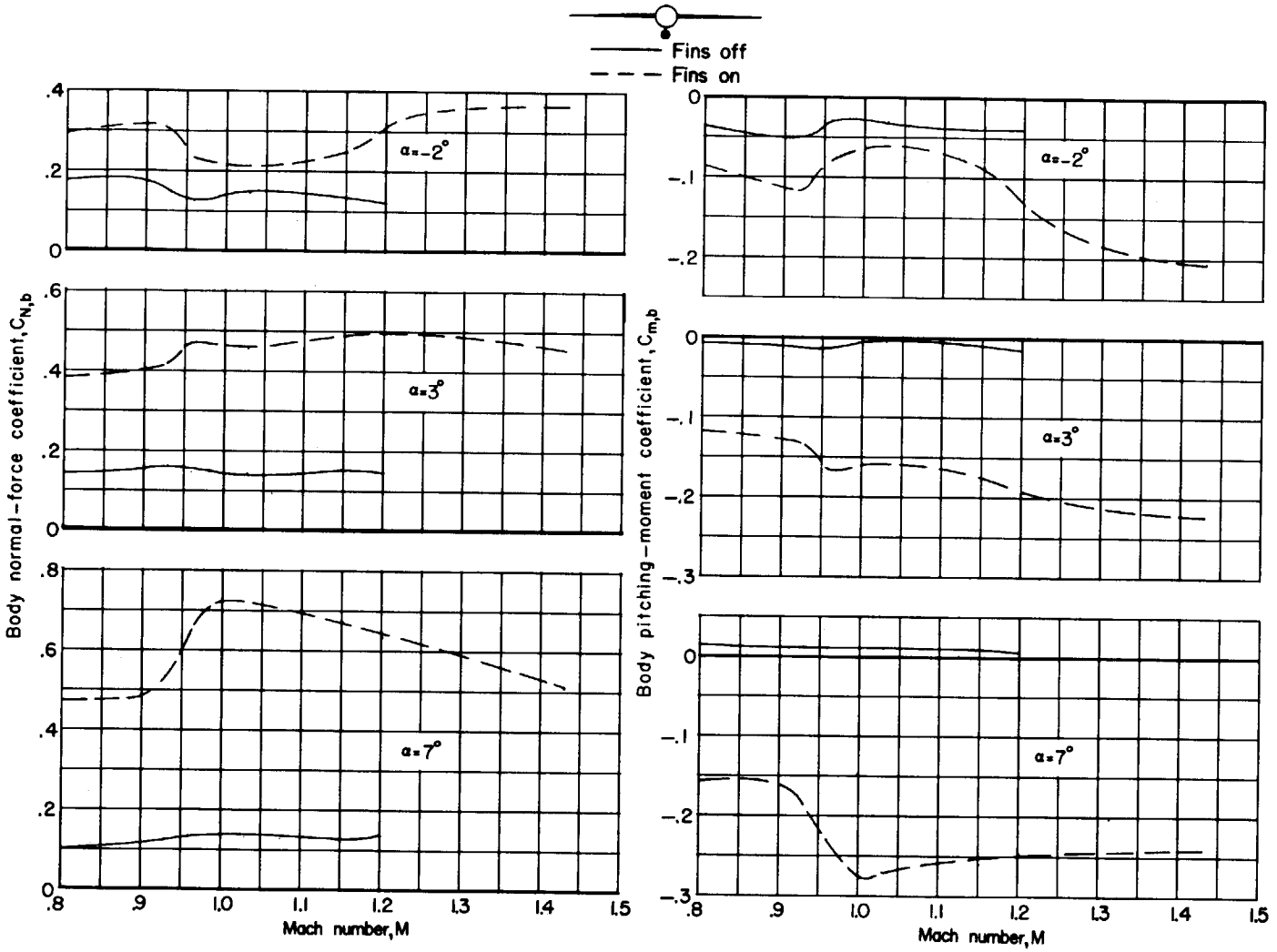

Figure 18.- Variation with Mach number of the forces and moments on the finned and unfinned body pylon-mounted beneath the fuselage at $\alpha = -2^{\circ}$, 3°, and 7°.

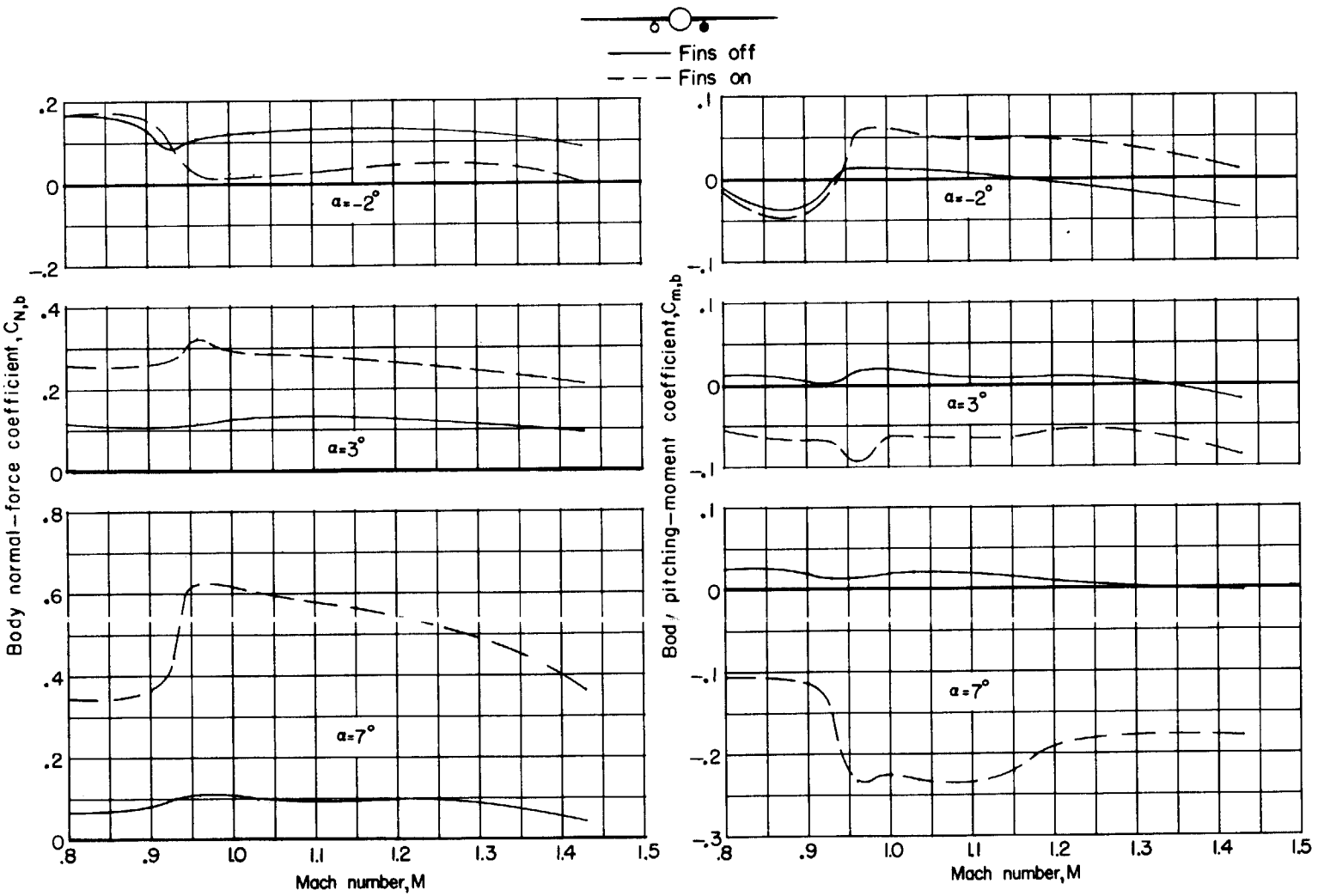

Figure 19.- Variation with Mach number of the forces and moments on the finned and unfinned body pylon-mounted beneath the left wing at $\alpha = -2^{\circ}$, 3°, and 7°.

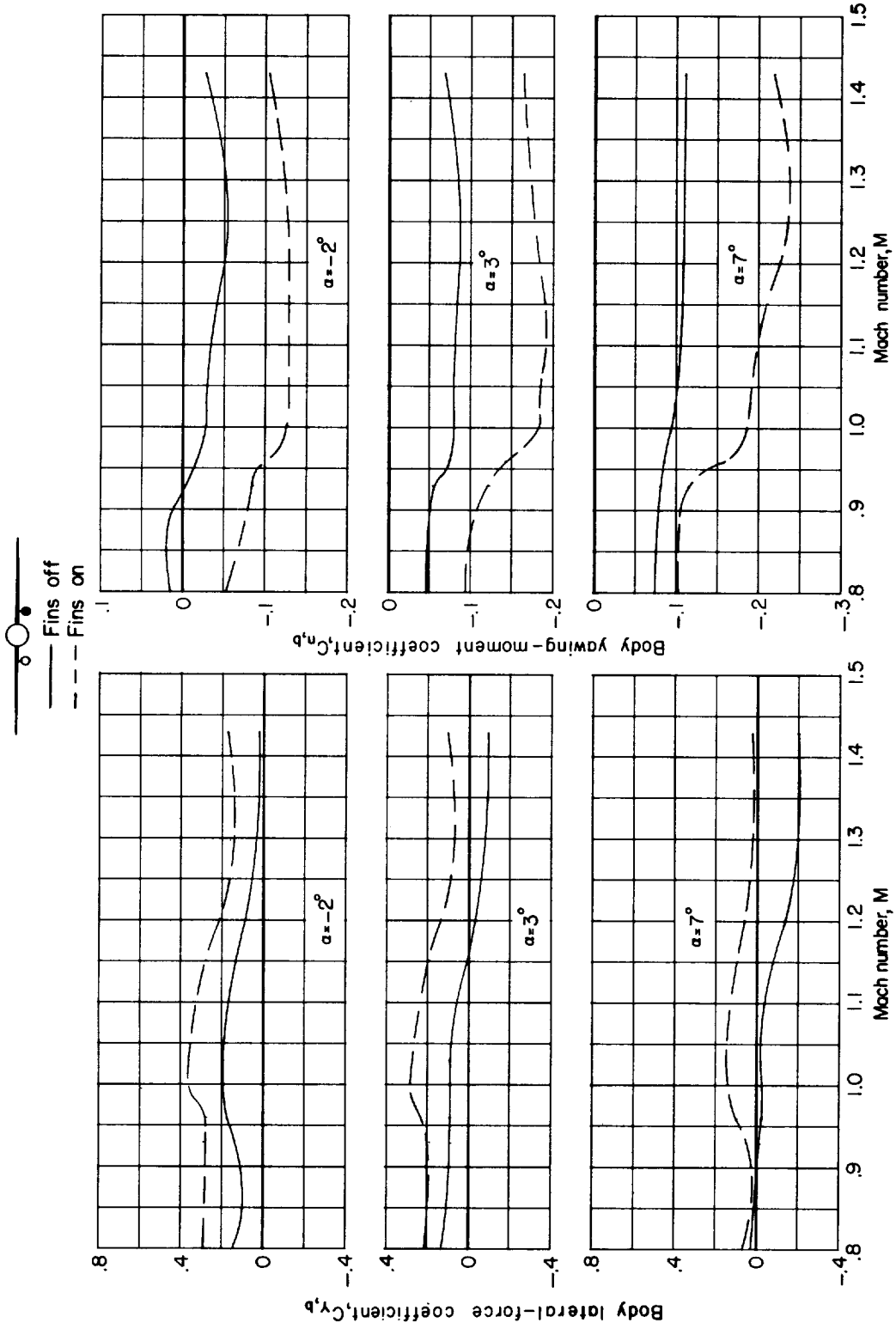

Figure 19.- Concluded.

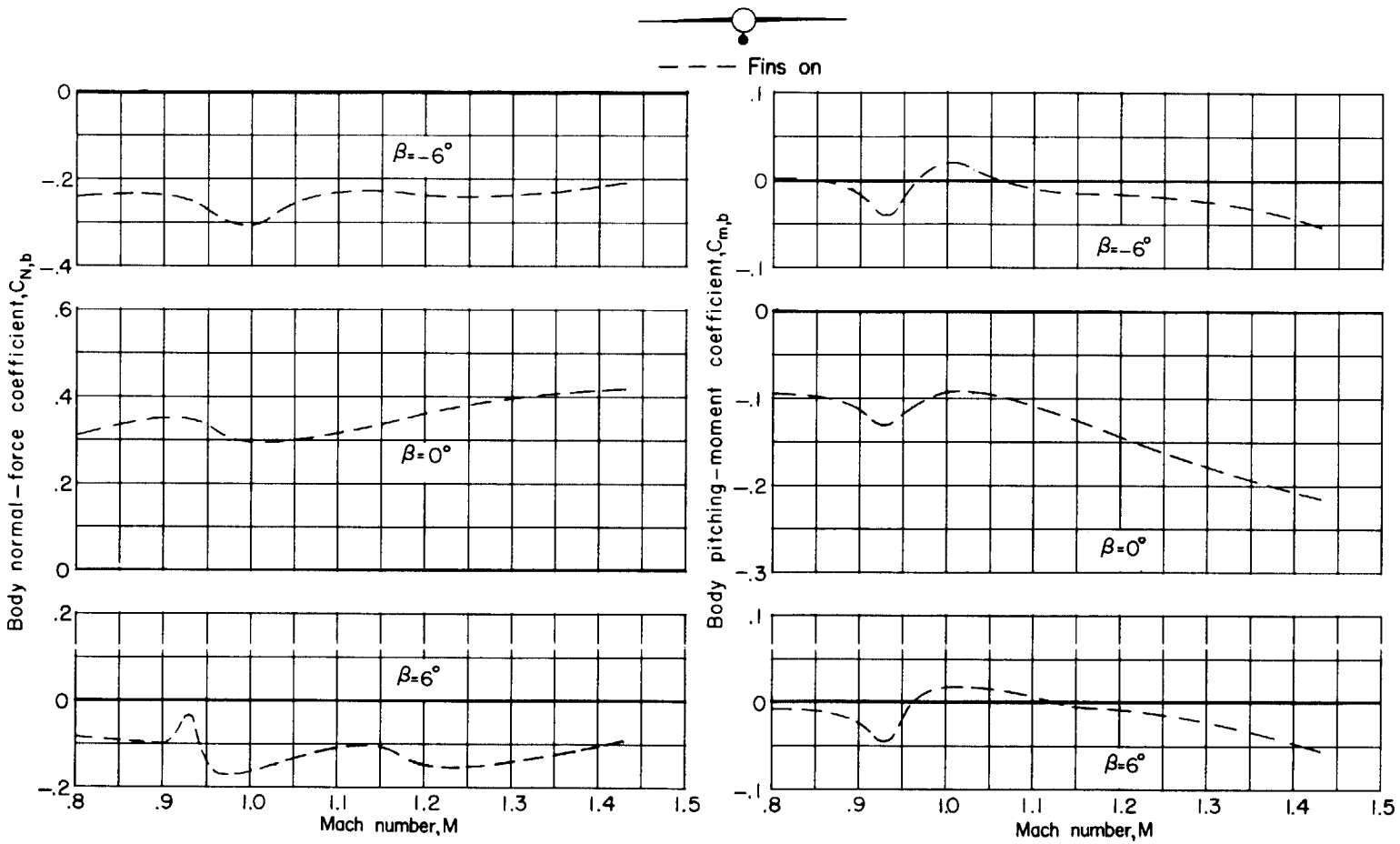

(a) $\alpha \approx -0.2°$.

Figure 20.- Variation with Mach number of the forces and moments on the finned and unfinned body pylon-mounted beneath the fuselage at $\beta = -6°$, $0°$, and $6°$.

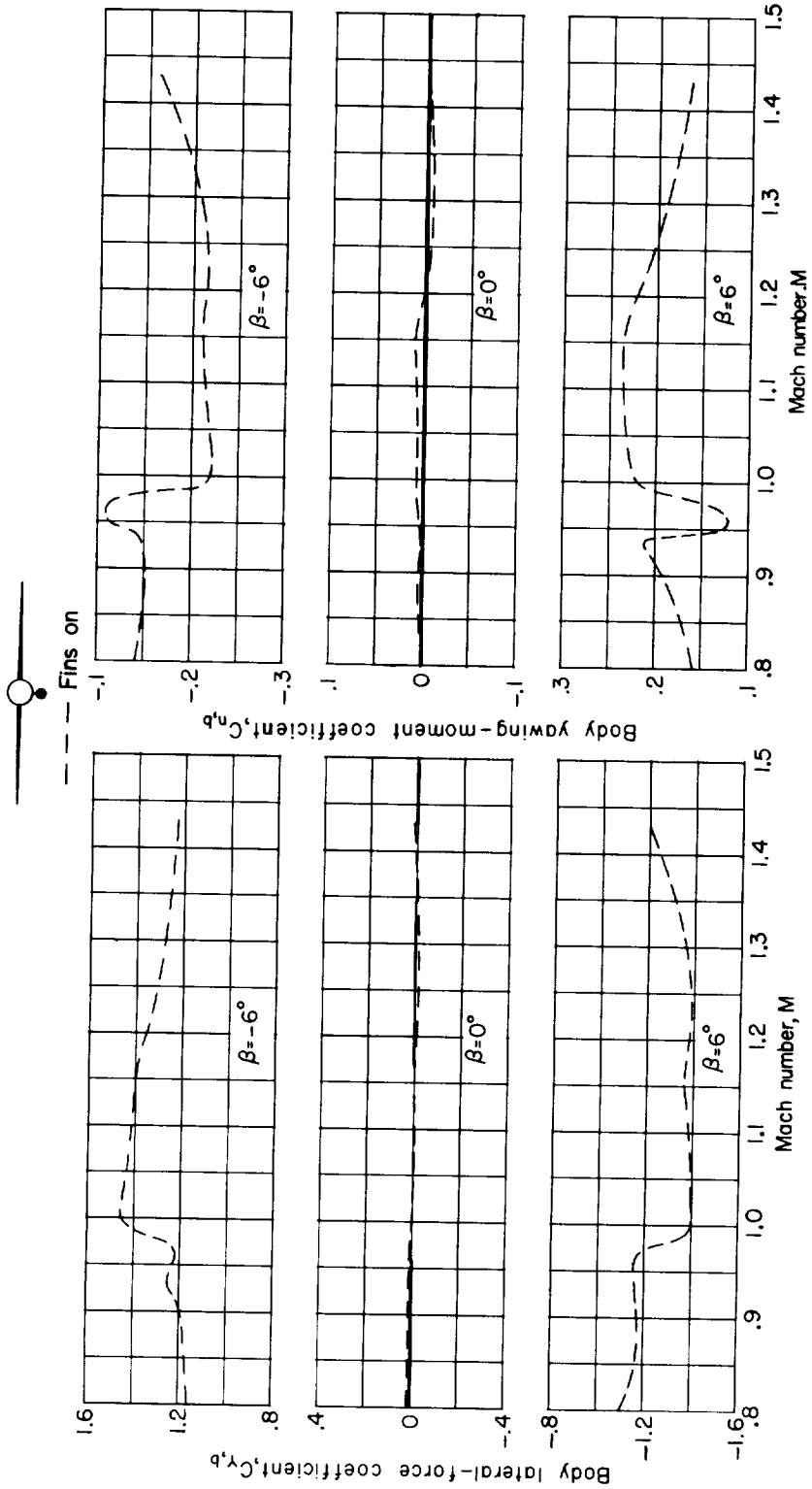

(a) $\alpha \approx -0.2^{\circ}$.- Concluded.

Figure 20.- Continued.

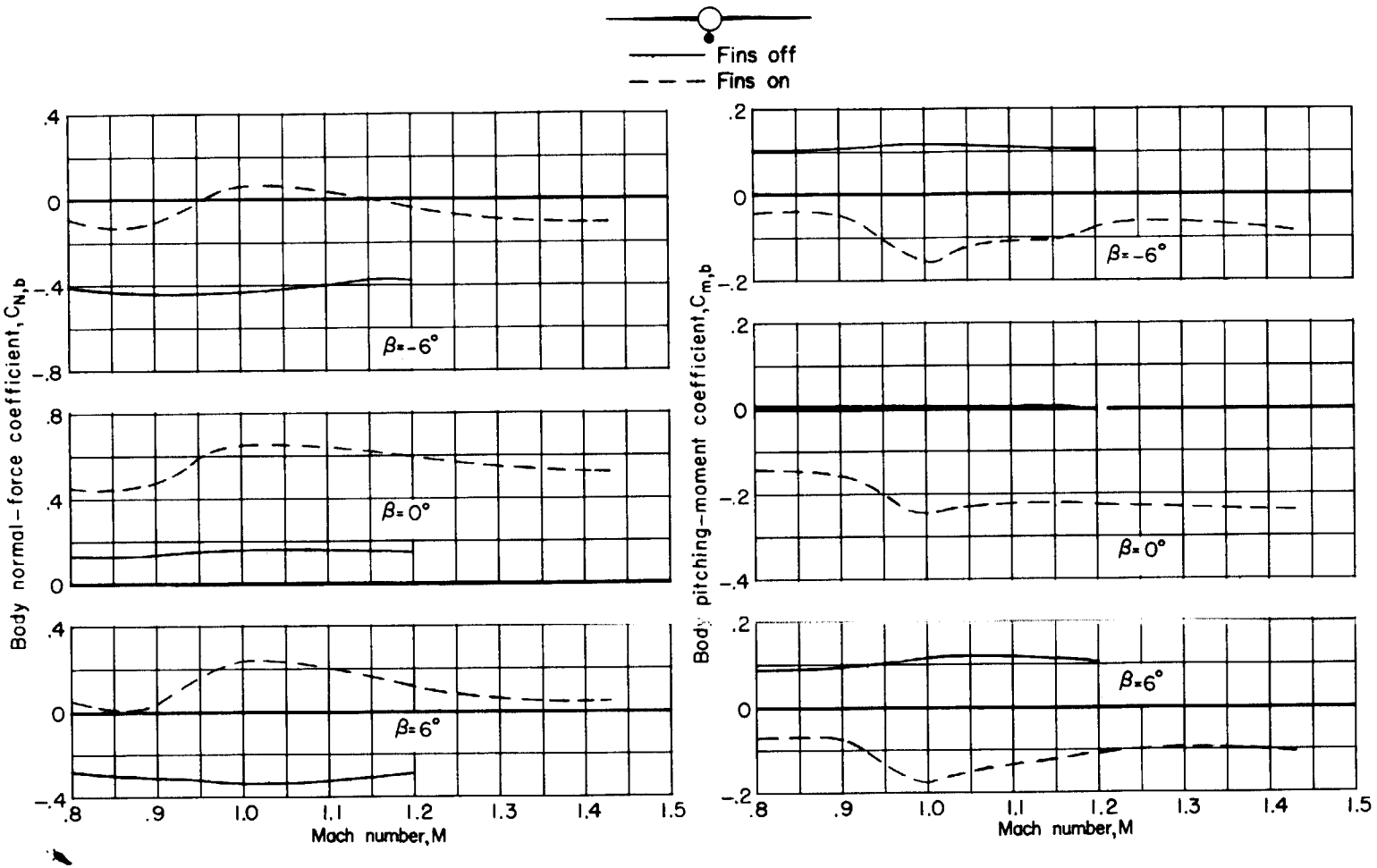

(b) $\alpha \approx 5.7^{\circ}$.

Figure 20.- Continued.

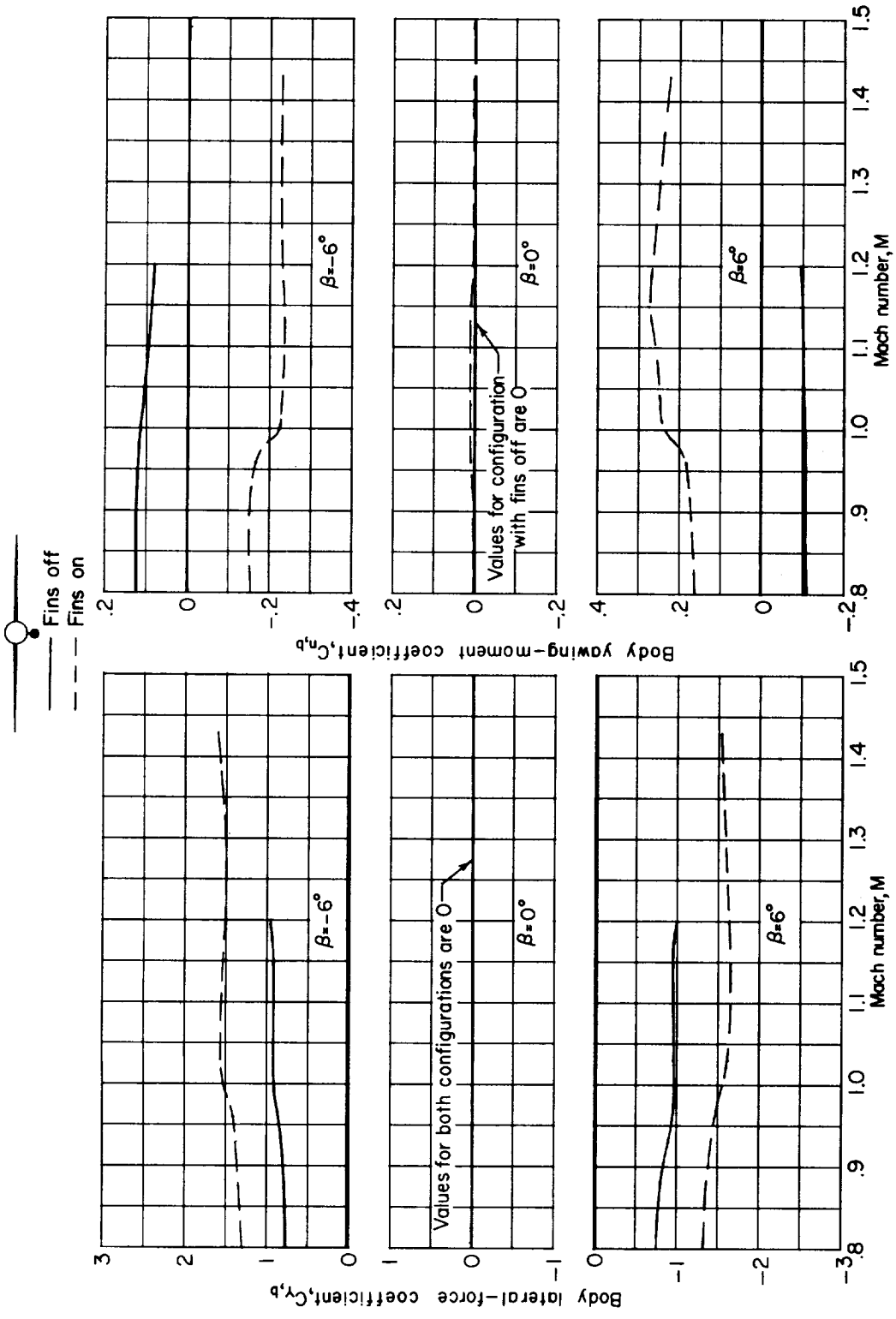

(b) $\alpha \approx 5.7°$. Concluded.

Figure 20.- Concluded.

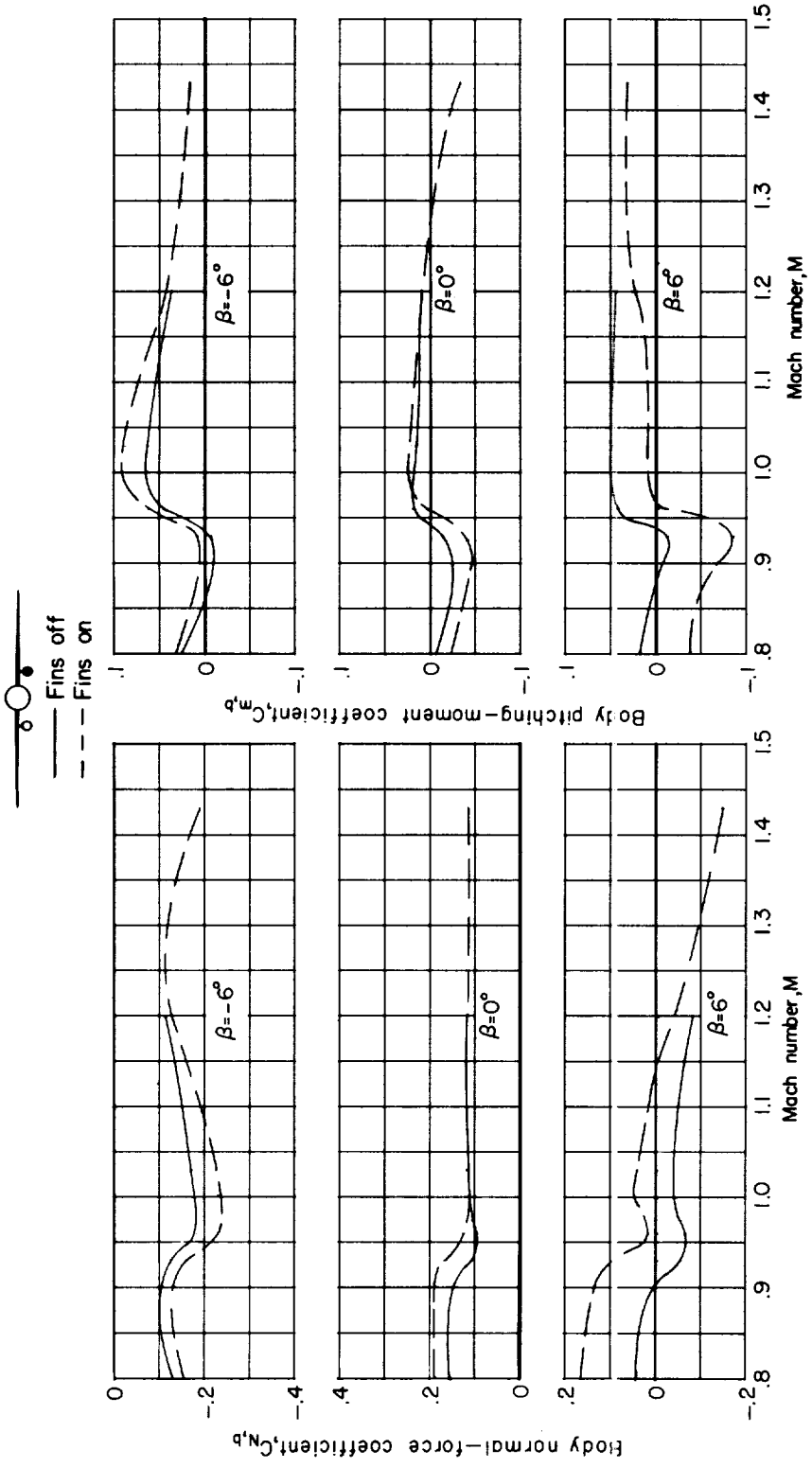

(a) $\alpha \approx -0.2^{\circ}$.

Figure 21.- Variation with Mach number of the forces and moments on the finned and unfinned body pylon-mounted beneath the left wing at $\beta = -6^{\circ}$, 0°, and 6°.

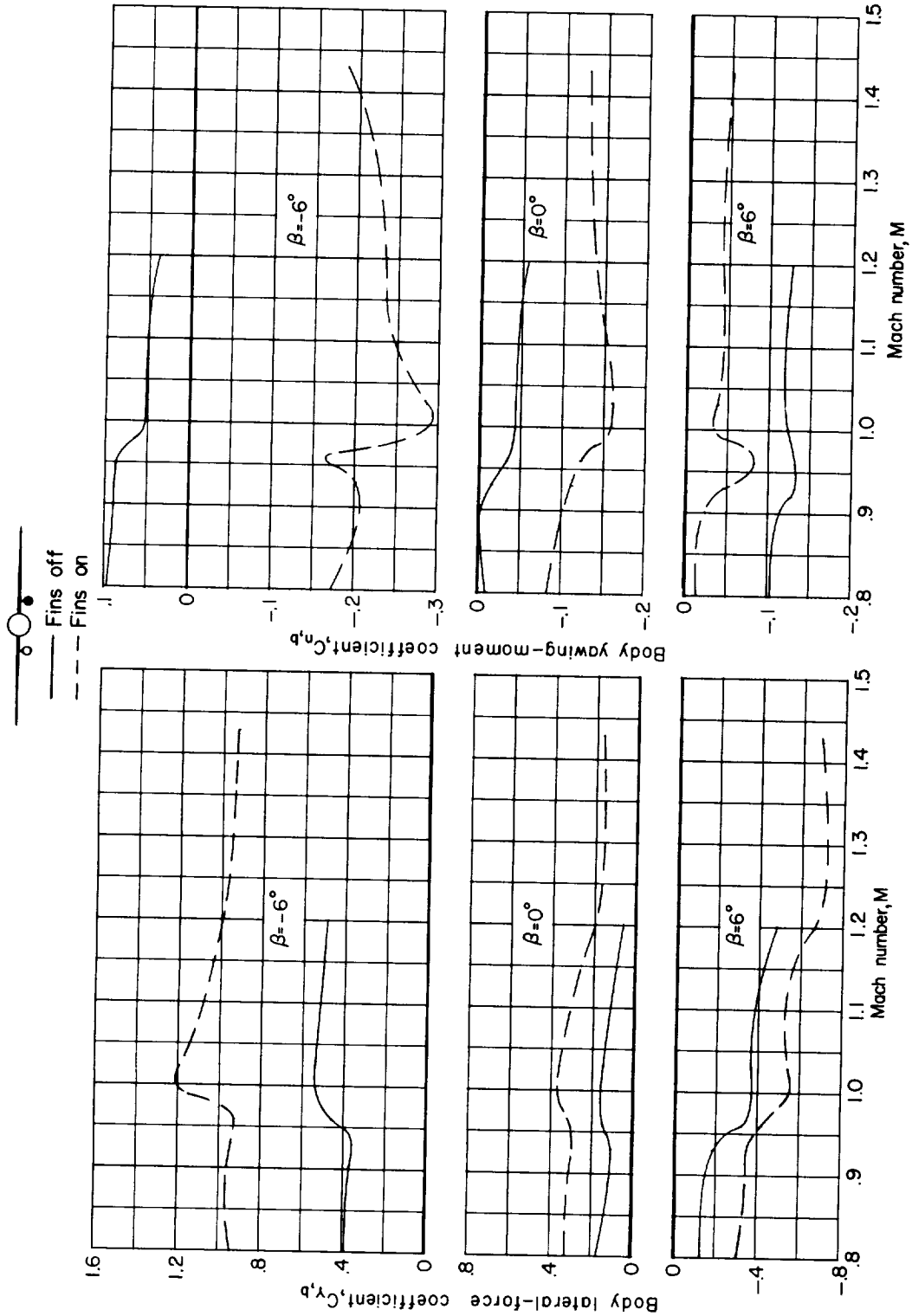

(a) $\alpha \approx -0.2^{\circ}$. Concluded.

Figure 21.- Continued.

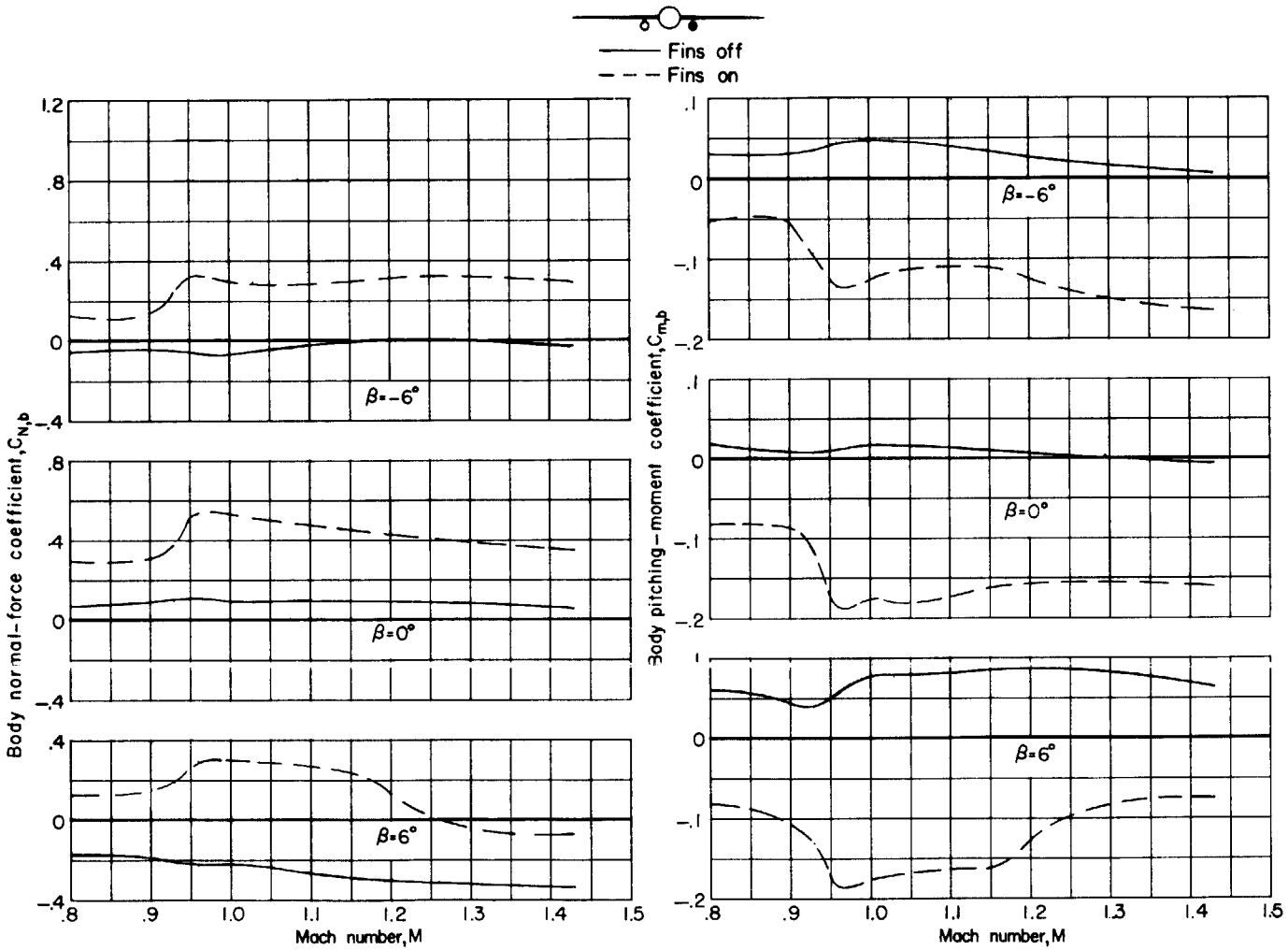

(b) $\alpha \approx 5.6^{\circ}$.

Figure 21.- Continued.

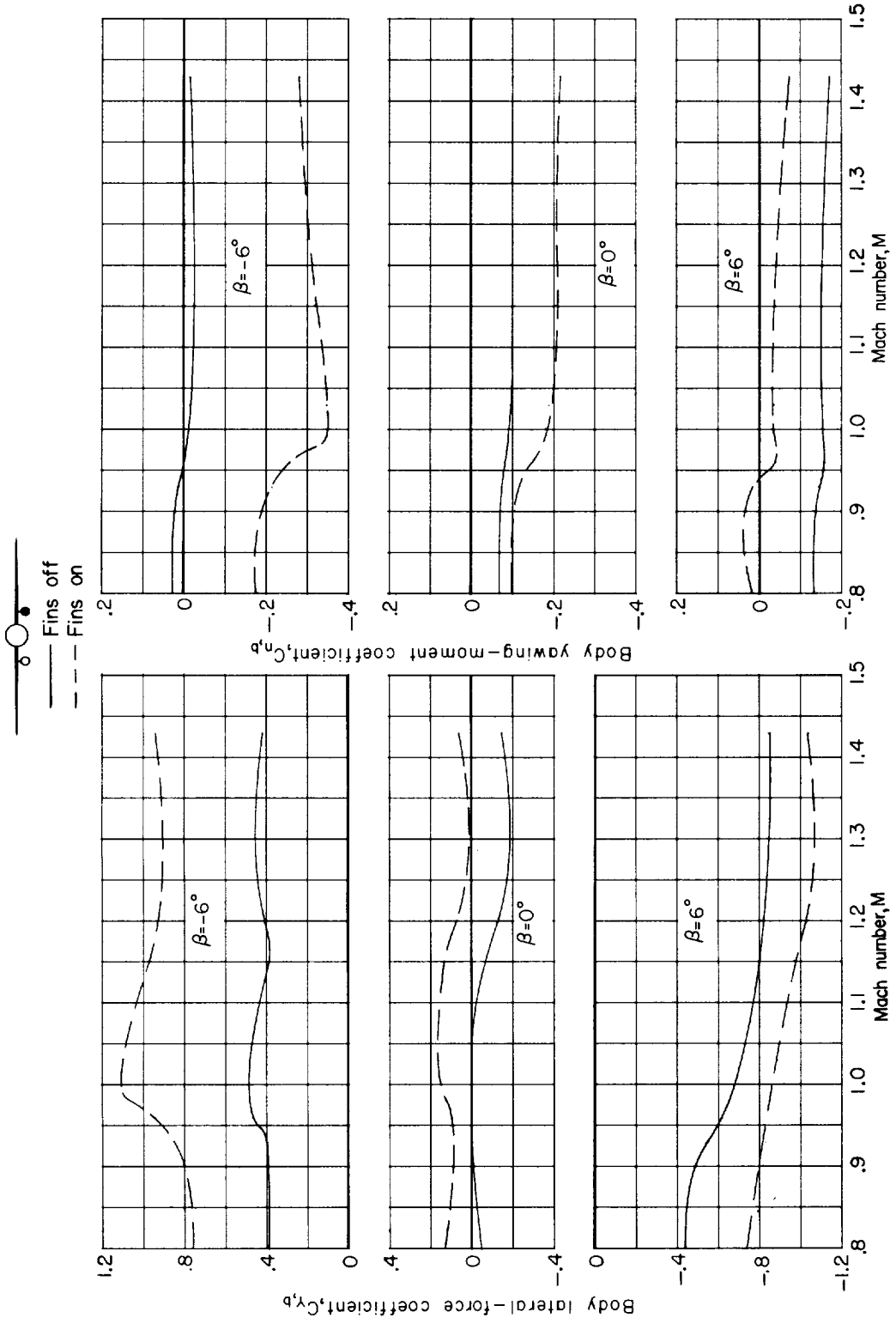

(b) $\alpha \approx 5.6°$. Concluded.

Figure 21.- Concluded.